COMMUNICATION

Check for updates

Defect chemistry of mixed ionic–electronic conductors under light: halide perovskites as a master example

Davide Moia (iD) *† and Joachim Maier (iD)

Shining light on a mixed ionic–electronic conductor induces variations in both its electronic and ionic behaviors. While optoelectronic processes in semiconductors with negligible ionic conductivities are well understood, the role of mobile ions in photoactive mixed conductors, such as hybrid halide perovskites, is largely unexplored. Here, we propose a model addressing this problem, combining optoelectronics and optoionics. Using methylammonium lead iodide (MAPI) as a model material, we discuss the expected influence of optical bias on the charge carrier chemistry of mixed conductors under steady-state conditions. We show that changes in the concentration of ionic defects under light with respect to the dark case are a direct consequence of their coupling to electrons and holes through the component chemical potential (iodine in the case of MAPI) and the electroneutrality condition. Based on the trend in the quasi-Fermi level splitting in the mixed conductor, we emphasize implications of controlling point defect chemistry for the function and performance optimization of solar energy conversion devices, including those based on halide perovskites. Lastly, we show that, in the presence of multiple redox reactions mediating the ionic and electronic quasi-equilibrium, either positive or negative changes in the ionic defect pair chemical potential can be obtained. These findings indicate the intriguing possibility to increase or reduce ionic defect concentrations in mixed conductors through exposure to light.

New concepts

We present a model describing the defect chemistry of mixed conductors under light. The evaluation of the electronic and ionic charge carrier quasi-equilibrium upon illumination reveals light-induced ionic phenomena resulting from the interaction of such charge carriers with each other as well as with the gas phase. Using representative input parameters for iodide perovskites, we identify and explore the key kinetic parameters that control the mixed conductor's electronic and ionic response under light, emphasizing the importance of understanding defect chemical effects in the optimization of solar cells. We demonstrate that light-induced enhancement and reduction in ionic defect concentrations in these materials are a natural consequence of the electroneutrality condition and the coupling between ionic and electronic charge carriers through the component chemical potential. The prediction that light can induce changes in stoichiometry and/or overall enhancement or reduction in ionic defect concentrations has direct consequences for any photoelectrochemical device using mixed conductors that include redox-active ionic defects, such as perovskite solar cells. More broadly, this work points to new avenues in the development of photodriven stoichiometry control in mixed conductors as well as in the design of materials and devices where defect concentrations can be either enhanced or reduced by light.

Introduction

Understanding the effect of illumination on the properties of mixed ionic–electronic conductors represents a basic yet largely unanswered question in the field of materials science. Addressing this question has fundamental implications not only for existing photoelectrochemical devices, including solar cells and other energy conversion and storage systems, but also for the development of novel devices in the fields of catalysis, computing and beyond.

Max Planck Institute for Solid State Research, Heisenbergstraße 1, 70569 Stuttgart, Germany. E-mail: moia.davide@gmail.com
† Current address: Fluxim AG, Katharina-Sulzer-Platz 2, 8400 Winterthur, Switzerland.

The description of a photoelectrochemical system can be greatly simplified, if the condition of local equilibrium applies during its operation. It is then straightforward to define the thermodynamic state at each position in the device through parameters including the (electro)chemical potential for all charged and neutral species, stoichiometry, defect formation energies to name a few. The quantification of such parameters is still possible locally, when a chemical or electrochemical bias applied across the system induces gradients in the electrochemical potentials of electrons and ions (*e.g.* batteries or fuel cells under operation).[1]

In many cases of interest, the applied bias leads to deviation from local equilibrium. This is the case for semiconductors used in solar cells, where light absorption leads to local non-equilibrium between the electronic charges populating different energy bands.[2,3] Local non-equilibrium can also arise in the

dark, when a voltage bias is applied to such devices, due to injection selectivity of the contacts. A similar condition may, in principle, be obtained for different ionic defects, if the relevant sublattices are not at equilibrium with each other. The discussion of these situations can be addressed using quasi-equilibrium arguments, where different defects related to a specific component (*e.g.* conduction band electrons, e′, and valence band holes, h•, related to electrons e⁻) are described by separate occupation statistical functions and separate quasi-electrochemical potentials. This treatment is applicable if equilibration within each charge carrier population occurs at a much faster rate than any of the reactions in which such carriers are involved.

In general, given a material component or defect j, its quasi-electrochemical potential can be expressed in the form:

$$\tilde{\mu}_j^* = \tilde{\mu}_{j,\text{eq}} + \delta\tilde{\mu}_j, \tag{1}$$

where the equilibrium value and the deviation from it are indicated as $\tilde{\mu}_{j,\text{eq}}$ and $\delta\tilde{\mu}_j$, respectively.

While these are not simple energies, the quasi-electrochemical potentials of electronic charges are often discussed in terms of quasi-Fermi energies for electrons, E_{Fn}, and for holes, E_{Fp}, each referring to separate Fermi–Dirac statistics.[4,5] The resulting quasi-Fermi level splitting QFLS = $E_{\text{Fn}} - E_{\text{Fp}}$ can then be expressed as the combined electron–hole chemical potential change according to

$$\text{QFLS} = \delta\tilde{\mu}_{\text{e}'} + \delta\tilde{\mu}_{\text{h}}^\bullet, \tag{2}$$

and it can be used to quantify the "degree of local electronic non-equilibrium." Assuming a dilute situation, the product of the concentrations of electrons (n) and holes (p) is related to the QFLS, as described by the modified mass-action law,

$$np = K_{\text{B}} \exp\left(\frac{\text{QFLS}}{k_{\text{B}}T}\right) \tag{3}$$

where k_{B} is the mass action constant of e′–h• thermal generation and recombination, often written as n_{i}^2; k_{B} and T are Boltzmann's constant and temperature. At equilibrium ($n = n_{\text{eq}}$ and $p = p_{\text{eq}}$), this expression reduces to the conventional mass-action law $n_{\text{eq}}\,p_{\text{eq}} = k_{\text{B}}$ (QFLS = 0). For situations where all ionic defects are immobile, as is the case at room temperature for most semiconductors in solar cells, eqn (3) reflects the local quasi-equilibrium in the material under bias.

In a mixed ionic–electronic conductor, where electronic and ionic charges are mobile, the equilibrium situation is defined by a more complex set of equations. These are derived from the mass-action laws involving ionic and electronic defects, coupled through the chemical potential (partial pressure) of components associated with the relevant mobile ions.[6–8] Under bias, the coupling between electrons and ions in these materials means that the ionic situation can vary too, even when a purely optoelectronic excitation is considered.

Hybrid halide perovskites are a relevant example to this question. These materials are used as active layers for high performance optoelectronic devices while also showing significant ionic conduction even at room temperature.[9,10] In methylammonium lead iodide (MAPbI₃ or MAPI), a reference compound for hybrid perovskite photovoltaics, migration of iodide defects (specifically vacancies) enables access to its defect chemical behavior by varying the iodine partial pressure in the system ($P(I_2)$).[3,11,12] While the characterization of MAPI under equilibrium conditions is becoming established, the study of its properties under light has resulted in numerous peculiar observations including anomalies in mass transport, phase stabilities and mechanical properties. Many of them have been interpreted in terms of coupled ionic–electronic effects and are still matter of debate.[13–18]

Other "unusual" photoelectrochemical effects in various mixed conductors have also been interpreted based on interactions between photogenerated electronic carriers and ionic defects (photoionic or optoionic effects).[14,19–22] The study of light effects in strontium titanate (STO)[19] highlighted the enhanced kinetics of oxygen incorporation in the material by (above bandgap) illumination, explained by the electronic contribution to the exchange reaction. While these investigations showed the effect of light on the surface kinetics, later reports discussed stoichiometric changes in conductivity on illumination for MAPI or STO.[14,22–24] Light effects have also been reported as far as the grain boundary resistance (for Gd-doped ceria) is concerned.[21]

All these reports point towards fundamental interactions between electronic and ionic charges, which, upon a drastic increase of electronic charge carrier concentration under light, inevitably modify the ionic equilibrium too. While these studies have suggested models that could explain the experimental results, systematically treating the quasi-equilibrium behavior of mixed conductors under light bias means entering largely unknown territory.

Fig. 1 displays the research question of this study (top schematics): Given a mixed conductor (*e.g.* MAPI) and the point defect model describing its equilibrium situation (*e.g.* $P(I_2)$ dependence of defect concentrations, *cf.* dashed lines in Fig. 3), how to describe the situation under light? This question is addressed at the bottom of Fig. 1 based on the generalized energy level representation, which considers the standard partial (free) energy levels and electrochemical potentials associated with the electronic and the ionic (here iodide only, for simplicity) defects.[7] In the diagram, the position of the electrochemical potentials $\tilde{\mu}_{\text{I}^-}$ and $\tilde{\mu}_{\text{e}^-}$ relative to the standard potentials ($\tilde{\mu}^0$) determines the concentrations of iodide vacancies and interstitials, $V_{\text{I}}^\bullet$ and I_{i}', and electrons and holes, e′ and h•, respectively.

The chemical potential of iodine in MAPI corresponds to $\mu_{\text{I,MAPI}} = \tilde{\mu}_{\text{I}^-} - \tilde{\mu}_{\text{e}^-}$ and, at equilibrium, it is equal to the given chemical potential of iodine in the gas phase, $\mu_{\text{I,MAPI,eq}} = \frac{1}{2}\mu_{\text{I}_2,g}$. Taking the former relationship for granted also for the nonequilibrium situation implies that changes in the electrochemical potential of electronic charges due to an applied bias result in changes in the iodine and/or iodide (electro)chemical potential in the material. The situation is complicated by the fact that electrons and holes are now not in equilibrium, as indicated by the two quasi-electrochemical potentials $\tilde{\mu}_{\text{e}'}^*$ and $\tilde{\mu}_{\text{h}}^*$. Furthermore, ionic defect concentrations may also vary under bias. Therefore, the straightforward definition of $\mu_{\text{I,MAPI}}$ used above is no longer applicable (Fig. 1b).
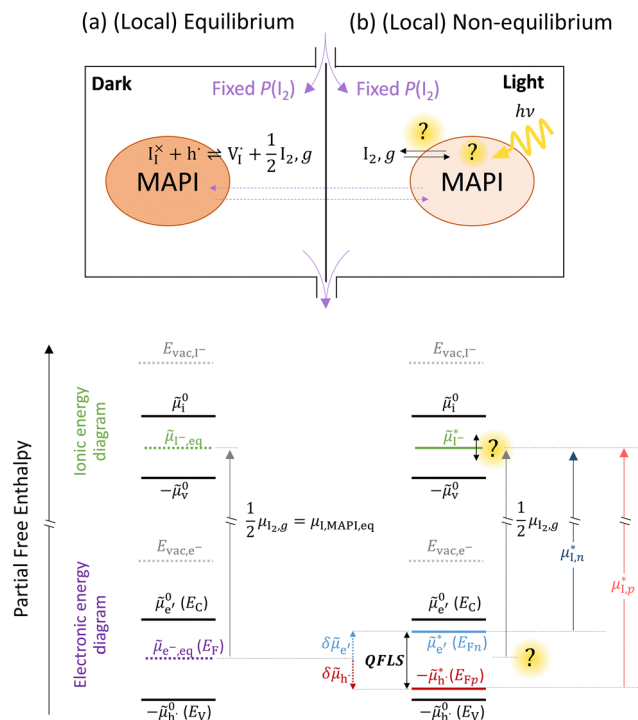
Fig. 1 Understanding the effect of light on the ionic and electronic properties of a mixed ionic–electronic conductor. (Top) Schematics of a mixed conductor (in this case MAPI) and (bottom) generalized energy diagram including the electronic and ionic (iodide) defect energy levels (a) under equilibrium and (b) under illumination (out-of-equilibrium). In the top schematics, the two MAPI samples are at equilibrium with each other only as far as the exchange of iodine is concerned (see dashed purple arrows). Specifically, they do not exchange radiation with each other. The $P(I_2)$ dependence of the defect concentration under equilibrium can be evaluated based on mass-action laws and the exchange reaction with iodine in the gas phase. Such dependence is more complex for the quasi-equilibrium situation under light. In other words, while in (a) the relationship between the electronic and the ionic electrochemical potentials and the chemical potential of iodine is straightforward $\left(\frac{1}{2}\mu_{I_2,g} = \tilde{\mu}_{I^-,eq} - \tilde{\mu}_{e^-,eq}\right)$, in (b) such relationship is not clearly defined, even assuming a single value for $\tilde{\mu}_{I^-}^*$ (quasi-chemical potentials of iodine defined as $\mu_{I,p}^* = -\tilde{\mu}_{V_I^\bullet}^* + \tilde{\mu}_{h^\bullet}^*$ and $\mu_{I,n}^* = -\tilde{\mu}_{V_I^\bullet}^* - \tilde{\mu}_{e'}^*$, where, $\tilde{\mu}_{I^-}^* = -\tilde{\mu}_{V_I^\bullet}^*$).

disorder in a mixed ionic–electronic conductor and the component quasi-equilibrium with the gas phase, with the equations associated with the generation and recombination of electronic charge carriers. We present results obtained using MAPI as a model system and illustrate the expected trend in defect concentrations under illumination. In the framework of quasi-equilibrium considerations, we discuss implications of these results for the study of photoactive mixed conductors and their use in photoelectrochemical devices for energy conversion. By exploring the effect of relevant kinetic and thermodynamic parameters on the material's defect chemistry under light, special emphasis is given to the predicted possibility to control (increase but also decrease) ionic defect concentration using light.

The model

The model presented in this study accounts for internal defect reactions occurring in a mixed ionic–electronic conductor exposed to light and for the exchange quasi-equilibria with the gas phase. The model represents the simplest possible problem that allows for a complete evaluation of the charge carrier chemistry in mixed conductors under light resulting from all the relevant and interacting ionic and electronic processes. For a discussion of the defect chemistry of mixed conductors under equilibrium conditions, we refer the reader to previous studies.[7,8] Below, we describe the model in detail (see also schematic representations of the model in Fig. 2 and in Section 1 of the SI).

We refer to a pore-free thin film of MAPI exposed to a set illumination condition and to a fixed iodine partial pressure, $P(I_2)$, at room temperature. The results and trends presented in the next section are relevant not only to halide perovskites but also to any photo-active mixed conductor, provided that the appropriate variations in chemical and physical properties are accounted for. We assume the film to be thin enough, so that, when exposed to light, the photogeneration rate can be assumed constant throughout the film volume. We also focus on a reaction-limited model, where transport is fast enough, resulting in homogeneous concentration profiles in the film for all mobile defects. Because of the complexity of including all possible defects in MAPI and the reactions involving them, we limit our analysis to the study of iodine and iodide defects, interstitial and vacancies. Regarding the solid–gas exchange of iodine, we focus on processes that involve neutral iodine defects only $(I_i^\times, V_I^\times)$, while other reactions may also contribute to the real system.

The relevant reactions are described in Table 1 and schematically represented in Fig. 2. For reaction r, the expressions for the rate of forward and backward reactions used in the kinetic model, $\vec{R}_r$ and $\overleftarrow{R}_r$, are defined based on rate constants $\left(\vec{k}_r \text{ and } \overleftarrow{k}_r\right)$ and the concentration of the relevant reactants. We indicate the mass-action constant K_r, defined based on the equilibrium concentrations of the relevant defects $\left(K_r = \vec{k}_r/\overleftarrow{k}_r\right)$.[23] On a first order approximation, and based on the quasi-equilibrium framework, we can assume that the value of the rate constants for the forward

One way to describe this situation involves the definition of iodine quasi-chemical potentials, such as $\mu_{I,p}^* = -\tilde{\mu}_{V_I^\bullet}^* + \tilde{\mu}_{h^\bullet}^*$ and $\mu_{I,n}^* = -\tilde{\mu}_{V_I^\bullet}^* - \tilde{\mu}_{e'}^*$ (assuming $-\tilde{\mu}_{V_I^\bullet}^* = \tilde{\mu}_{I_i'}^* = \tilde{\mu}_{I^-}^*$), which would be identical at equilibrium but different otherwise (see also discussion by Kim *et al.*[14] and Viernstein *et al.*[23] for halide and oxide perovskites, respectively). Their relationship with the chemical potential of iodine in the gas phase is then kinetically determined. Further complexity is introduced by the influence of mobile ionic defects on the optoelectronic quasi-equilibrium (*e.g.* the electron–hole recombination rate).[25–29] A model to evaluate such interplays and to predict the electronic and ionic charge carrier concentrations as a function of the component partial pressures (*e.g.* $P(I_2)$ in MAPI) in a mixed conductor is currently missing.[30]

Here, we address the problem shown in Fig. 1 by coupling the defect chemical relationships describing ionic and electronic

Table 1 Defect chemical reactions used in this study to describe the electronic and ionic disorder in MAPI under constant $P(I_2)$ at equilibrium in the dark or under light. The expressions for the forward and backward rates are shown, as well as the equilibrium (eq) mass-action laws and the pseudo mass-action laws for the nonequilibrium case. The terms in () in the Defect reaction column are used as labels to the defect reactions (cf. Fig. 2; B = bandgap excitation, $\bar{F}$ = anti-Frenkel ionic defects, $\bar{F}^\times$ = neutral anti-Frenkel ionic defects, sg = solid–gas exchange, n = electrons, p = holes, v = vacancies, i = interstitials). [] indicates defect concentrations. E_g, $\Delta G_{\bar{F}}^0$ and $\Delta G_{\bar{F}^\times}^0$ are the standard free enthalpy of reactions (B), ($\bar{F}$) and ($\bar{F}^\times$)

Reaction	Defect reaction	Rates	(Pseudo) mass-action law
Electronic	$h\nu \rightleftarrows e' + h^\bullet$ (B) (radiative case)	$G = G_{ext} + \sum_k G_{th,k}$ $R = \sum_k R_k$ k = rad, SRH, Aug, I	$K_B = n_{eq}p_{eq} \propto \exp\left(-\frac{E_g}{k_B T}\right)$ $\left(\text{light: } np = K_B \exp\left(\frac{QFLS}{k_B T}\right)\right)$
Ionic (anti-Frenkel disorder)	$V_i^\times + I_I^\times \rightleftarrows I_i' + V_I^\bullet$ ($\bar{F}$)	$\vec{R}_{\bar{F}} = \vec{k}_{\bar{F}}$ $\overleftarrow{R}_{\bar{F}} = \overleftarrow{k}_{\bar{F}}[I_i'][V_I^\bullet]$	$K_{\bar{F}} = [I_i']_{eq}[V_I^\bullet]_{eq} \propto \exp\left(-\frac{\Delta G_{\bar{F}}^0}{k_B T}\right)$ $\left(\text{light: } [I_i'][V_I^\bullet] = K_{\bar{F}} \exp\left(\frac{\Delta\mu_{\bar{F}}}{k_B T}\right)\right)$
Ionic (neutral defect disorder)	$V_i^\times + I_I^\times \rightleftarrows I_i^\times + V_I^\times$ ($\bar{F}^\times$)	$\vec{R}_{\bar{F}^\times} = \vec{k}_{\bar{F}^\times}$ $\overleftarrow{R}_{\bar{F}^\times} = \overleftarrow{k}_{\bar{F}^\times}[I_i'][V_I^\bullet]$	$K_{\bar{F}^\times} = [I_i^\times]_{eq}[V_I^\times]_{eq} \propto \exp\left(-\frac{\Delta G_{\bar{F}^\times}^0}{k_B T}\right)$ $\left(\text{light: } [I_i^\times][V_I^\times] = K_{\bar{F}^\times} \exp\left[\frac{\Delta\mu_{\bar{F}^\times}}{k_B T}\right]\right)$
Redox (interstitial)	$I_i' + h^\bullet \rightleftarrows I_i^\times$ (p, i)	$\vec{R}_{p,i} = \vec{k}_{p,i}[I_i']p$ $\overleftarrow{R}_{p,i} = \overleftarrow{k}_{p,i}[I_i^\times]$	$K_{p,i} = \frac{[I_i^\times]_{eq}}{[I_i']_{eq}p_{eq}}$
	$I_i' \rightleftarrows I_i^\times + e'$ (n, i)	$\vec{R}_{n,i} = \vec{k}_{n,i}[I_i']$ $\overleftarrow{R}_{n,i} = \overleftarrow{k}_{n,i}[I_i^\times]n$	$K_{n,i} = \frac{[I_i^\times]_{eq}n_{eq}}{[I_i']_{eq}} = K_{p,i}k_B$
Redox (vacancy)	$V_I^\times + h^\bullet \rightleftarrows V_I^\bullet$ (p, v)	$\vec{R}_{p,v} = \vec{k}_{p,v}[V_I^\times]p$ $\overleftarrow{R}_{p,v} = \overleftarrow{k}_{p,v}[V_I^\bullet]$	$K_{p,v} = \frac{[V_I^\bullet]_{eq}}{[V_I^\times]_{eq}p_{eq}}$
	$V_I^\times \rightleftarrows V_I^\bullet + e'$ (n, v)	$\vec{R}_{n,v} = \vec{k}_{n,v}[V_I^\times]$ $\overleftarrow{R}_{n,v} = \overleftarrow{k}_{n,v}[V_I^\bullet]n$	$K_{n,v} = \frac{[V_I^\bullet]_{eq}n_{eq}}{[V_I^\times]_{eq}} = K_{p,v}K_B$
Iodine exchange (interstitial-mediated)	$I_i^\times \rightleftarrows V_i^\times + \frac{1}{2}I_2, g$ (sg, i)	$\vec{R}_{sg,i} = \vec{k}_{sg,i}[I_i^\times]$ $\overleftarrow{R}_{sg,i} = \overleftarrow{k}_{sg,i}P(I_2)^{\frac{1}{2}}$	$K_{sg,i} = \frac{P(I_2)^{\frac{1}{2}}}{[I_i^\times]_{eq}}$
Iodine exchange (vacancy-mediated)	$I_I^\times \rightleftarrows V_I^\times + \frac{1}{2}I_2, g$ (sg, v)	$\vec{R}_{sg,v} = \vec{k}_{sg,v}$ $\overleftarrow{R}_{sg,v} = \overleftarrow{k}_{sg,v}P(I_2)^{\frac{1}{2}}[V_I^\times]$	$K_{sg,v} = P(I_2)^{\frac{1}{2}}[V_I^\times]_{eq} = K_{sg,i}K_{\bar{F}^\times}$

and the backward reactions are the same under bias and under dark conditions. All relevant input parameters are shown in Section 1 of the SI.

Electronic properties

The electronic generation–recombination reaction involves multiple pathways[31] which can be described by means of net recombination terms $U_k = R_k - G_{th,k}$, where R_k and $G_{th,k}$ are the recombination and thermal generation rates associated with process k. The following expressions describe the radiative (k = rad), Shockley–Read–Hall (k = SRH) and the Auger (k = Aug) processes:

$$U_{rad} = k_{rad}(np - n_i^2) \quad (4)$$

$$U_{SRH} = \frac{np - n_i^2}{\tau_n(p + p_1) + \tau_p(n + n_1)} \quad (5)$$

$$U_{Aug} = \gamma_n(n^2p - n_{eq}^2p_{eq}) + \gamma_p(np^2 - n_{eq}p_{eq}^2) \quad (6)$$

Here, k_{rad} is the radiative constant, τ_n, τ_p, n_1 and p_1 are the capture time constant for electrons and holes and the concentration parameters describing the trap energy position, and γ_n and γ_p are the Auger coefficients. An additional term, U_I, is also considered, which refers to the net recombination rate deriving from the interaction of electrons and holes with the iodine defects (see eqn (12) below). In Table 1, the total generation rate G is the sum of the term G_{ext}, which corresponds to the external light bias, and all thermal generation terms, while the total recombination rate R is the sum of the rates associated with each recombination process.

Ionic properties

For the ionic situation, we concentrate on anti-Frenkel disorder[32–34] involving iodide vacancies and iodide interstitials (see also energy diagrams in Fig. 1). Being aware of the fact that Schottky disorder (iodine vacancies and methylammonium vacancies $V_I^\bullet$ and V_{MA}') is most likely the dominant ionic disorder in MAPI,[8,34] we assume
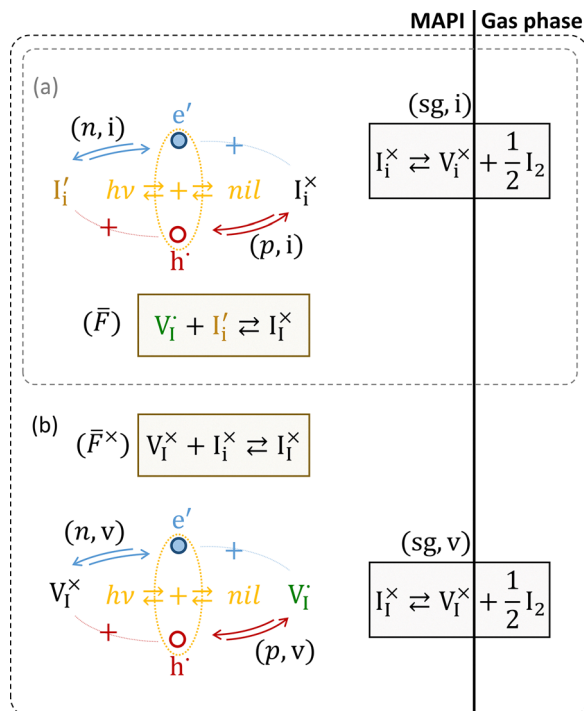
Fig. 2 A simple model to address the defect chemistry of a mixed conductor (here MAPI, or possibly other iodide conductors) under light. The schematic shows the coupling between optoelectronic reactions (generation and recombination) and the iodine (quasi)equilibrium of MAPI with the gas phase (sg is short for solid–gas). (a) Only iodide and iodine interstitials are redox-active ionic defects. (b) Both vacancies and interstitials are redox-active defects.

anti-Frenkel disorder to be dominant for the purpose of referring to a simple and straightforward model. The general conclusions of this study can be applied to the Schottky disorder case too.

Although the ionic defect concentrations are not directly influenced by illumination, the coupling *via* defect chemical reactions leads to a situation of quasi-equilibrium for the ionic situation, too. In this case, a quasi-electrochemical potential can be assigned to each ionic defect. Besides the mass-action constant associated with the anti-Frenkel disorder reaction at equilibrium, $K_{\bar{F}}$, we define a chemical potential of the anti-Frenkel ionic defects $\Delta\mu_{\bar{F}}$ to describe the nonequilibrium case, in analogy with QFLS for the electronic charges:

$$\Delta\mu_{\bar{F}} = \delta\tilde{\mu}_{I_i'} + \delta\tilde{\mu}_{V_I^\bullet}. \tag{7}$$

In section (a) of the Results, we discuss under what conditions an increase in electronic concentrations induces a shift in the ionic anti-Frenkel equilibrium, involving changes in the values of $[I_i']$ and $[V_I^\bullet]$, while maintaining $[V_I^\bullet][I_i'] = K_{\bar{F}}$, $\Delta\mu_{\bar{F}} = 0$ and $-\tilde{\mu}_{V_I^\bullet}^* = \tilde{\mu}_{I_i'}^* = \tilde{\mu}_{I^-}^*$. Other situations where the ionic disorder is taken out-of-equilibrium ($\Delta\mu_{\bar{F}} \neq 0$) are explored in section (b).

Finally, based on reaction $(\bar{F})$ shown in Table 1, we introduce the net-recombination term $U_{\bar{F}}$ for anti-Frenkel defect pairs. Assuming $U_{\bar{F}}$ to follow a bimolecular process, we write

$$U_{\bar{F}} = \overleftarrow{k}_{\bar{F}}[V_I^\bullet][I_i'] - \overrightarrow{k}_{\bar{F}} = \overleftarrow{k}_{\bar{F}}([V_I^\bullet][I_i'] - K_{\bar{F}}), \tag{8}$$

where $\overleftarrow{k}_{\bar{F}}$ and $\overrightarrow{k}_{\bar{F}}$ are the rate constants for the recombination and thermal generation of anti-Frenkel defect pairs. The term $\overleftarrow{k}_{\bar{F}}$ can be related to the Onsager radius $r_{\bar{F}}$ describing the recombination of (oppositely) charged defects as follows:

$$\overleftarrow{k}_{\bar{F}} = 4\pi D_{\bar{F}} r_{\bar{F}} \tag{9}$$

where $D_{\bar{F}}$ is the sum of the diffusion coefficients of the two defects participating in the recombination process.[35,36]
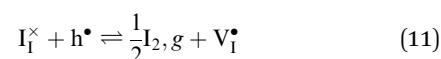
The analogous treatment of the neutral iodine defects is included in Table 1 together with the definition of parameters $K_{\bar{F}\times}$, $\Delta\mu_{\bar{F}\times}$. The net-recombination $U_{\bar{F}\times}$ can be defined similarly to eqn (8) (including $\overleftarrow{k}_{\bar{F}\times} = 4\pi D_{\bar{F}\times} r_{\bar{F}\times}$). In this work, we consider the solid–gas iodine exchange reaction as the only channel through which neutral iodine defects interact. This implies a net-recombination term of neutral defects:

$$U_{\bar{F}\times} = \vec{R}_{sg,i} - \overleftarrow{R}_{sg,i} = \overleftarrow{R}_{sg,v} - \vec{R}_{sg,v} \tag{10}$$

A contribution describing reactions of neutral defects in the bulk of the mixed conductor (reaction $(\bar{F}^\times)$ in Table 1, also shown in Fig. 2b) would be necessary when looking at other situations (*e.g.* encapsulated samples).

Iodine exchange and redox reactions

Redox activity of at least one of the charged ionic defects is necessary to mediate the component exchange reaction (more on this in Section 2 of the SI). At equilibrium, the following reaction can be used to describe the iodine exchange between MAPI and the gas phase.

$$I_I^\times + h^\bullet \rightleftharpoons \frac{1}{2}I_2, g + V_I^\bullet \tag{11}$$

Under light, electronic and ionic defects are no longer (necessarily) at equilibrium. Reaction (11) is therefore not sufficient to evaluate the quasi-equilibrium situation, and a kinetic model that includes the relevant redox reactions and iodine exchange reactions is required. The redox behavior of MAPI is complex, in terms of the range of relevant defects, oxidation states and redox reactions, and it may be different for the bulk and the surface.[25,26,37–40] Here, we select a simple problem which can serve as a basis for more accurate models. Specifically, we describe the interaction between ionic and electronic defects and the exchange of iodine at the solid–gas interface focusing on redox reactions where iodide interstitials or iodide vacancies interacting with either electrons or holes yield $I_i^\times$ or $V_I^\times$. Iodine in the gas phase is then either released from MAPI or incorporated in the structure *via* interaction with such neutral defects (Table 1 and Fig. 2). In the main text of this study, the neutral defects are assumed to be at equilibrium with each other and with the gas phase.

A key aspect in the discussion of how the redox reactions influence the defect concentration profiles concerns which of the reactions mediated by electrons or holes is dominant. To parameterize such aspects, we introduce the parameters $\Gamma_{I,i} = \vec{R}_{p,i}/\vec{R}_{n,i}$ and $\Gamma_{I,v} = \vec{R}_{p,v}/\vec{R}_{n,v}$ for reactions involving interstitials and

vacancies, respectively, to express the extent to which each reaction is more favorable when mediated by conduction band electrons or by valence band holes. The $\Gamma_{I,i}$ and $\Gamma_{I,v}$ parameters are evaluated in the equilibrium case and under the intrinsic composition condition, *i.e.* $n_{eq} = p_{eq} = n_i$ and $[V_I^\bullet]_{eq} = [I_i']_{eq} = K_{\bar{F}}^{1/2}$, occurring for $P(I_2) = P(I_2)_i$. Note that, at equilibrium, the $\Gamma_{I,i}$ and $\Gamma_{I,v}$ ratios are the same also when considering the backward reaction (*i.e.* $\vec{R}_{p,i}/\vec{R}_{n,i} = \overleftarrow{R}_{p,i}/\overleftarrow{R}_{n,i}$).

The trapping and release of electronic charge carriers from iodide defects can be treated using the Shockley–Read–Hall framework, as discussed above for U_{SRH} mediated by an immobile trap (see Section 2 of the SI). This also leads to an additional contribution to net recombination of electronic charge carriers U_I (*e.g.* the combination of $I_I' + h^\bullet \rightarrow I_i^\times$ and $I_i^\times + e' \rightarrow I_i'$ corresponds to the recombination process $h^\bullet + e' \rightarrow$ nil; the same would follow if we consider the reactions involving vacancy defects).

We can express the steady-state net recombination contribution due to all the redox reactions involving iodine defects as follows:

$$U_I = \sum_{w=i,v} \left(\overleftarrow{R}_{n,w} - \vec{R}_{n,w} \right) = \sum_{w=i,v} \left(\vec{R}_{p,w} - \overleftarrow{R}_{p,w} \right). \quad (12)$$

It is useful to parameterize the rates associated with mobile ion-mediated redox reactions with respect to other intrinsic rates. We define the parameters $\Gamma_{p,i}$ and $\Gamma_{n,v}$ as the normalized rate of hole trapping by an iodide interstitial and the normalized rate of electron trapping by an iodide vacancy, respectively. These rates are evaluated at equilibrium and at $P(I_2) = P(I_2)_i$, and they are normalized by the radiative recombination rate under the same condition (see Table 1 and Section 2 of the SI).

Steady-state solution

The equations resulting from the model described above are shown in Table 2. They reflect the fact that, at steady-state, no net mass-exchange occurs, the net recombination of electronic charges compensates for the external generation term, and the net recombination of ionic defects due to redox reactions is equal and opposite to their net recombination due to the anti-Frenkel reaction. By also considering the condition of electroneutrality, a system of six equations is obtained.

The analytical treatment becomes involved, requiring Brouwer approximations and additional simplification of the recombination terms to extract simple expressions for the $P(I_2)$ dependence of the charge carrier concentrations. We present

numerical solutions to the problem obtained by solving the equations in Table 2 using the MATLAB function 'fsolve' (software version R2019a).

Results and discussion

Single redox-active mobile ionic defect: ionic disorder at equilibrium

We start by considering scenario (a) in Fig. 2, where electronic charge carriers interact only with the interstitial defects $I_i^\times/I_i'$, while the rate constants associated with the $V_I^\times/V_I^\bullet$ reactions are negligibly small. Fig. 3a shows the ionic and electronic defect concentrations as a function of $P(I_2)$ for the equilibrium (dashed lines) and the situation under light (solid lines). We consider the (symmetrical) case of $\Gamma_{I,i} = 1$ (comparable rates for the redox reactions mediated by electrons or holes at $P(I_2)_i$), and a constant optical excitation of $\sim 10^{-3}$ suns equivalent. As expected, the electronic charge concentration is always larger under illumination than at equilibrium. Such an increase is accompanied by a narrowing of the intrinsic region which is the $P(I_2)$ range where ionic defects are larger in concentrations than electronic defects.

The concentration of iodide defects is perturbed under light too, as shown by the trend of $[V_I^\bullet]$ and $[I_i']$ deviating from the equilibrium profile, especially at low or high $P(I_2)$. Based on electroneutrality, a significant increase in $[V_I^\bullet]$ with respect to equilibrium at low $P(I_2)$ compensates for the large concentration of electrons obtained under light (see also $[I_i']$ and hole concentration at high $P(I_2)$). Interestingly, the profiles of $[V_I^\bullet]$ and $[I_i']$ still obey the anti-Frenkel equilibrium even under light, that is while their individual values are different from the equilibrium case, their product still corresponds to $K_{\bar{F}}$. The concentrations of the neutral ionic defects $[I_i^\times]$ and $[V_I^\times]$ vary with $P(I_2)$ according to the mass-action laws for the solid–gas exchange reactions (sg,i and sg,v in Table 1), whether the system is at equilibrium or under light (their profiles are omitted in all figures below).

The data illustrate that, depending on $P(I_2)$, illumination induces a net iodine uptake from or release to the gas phase compared to the equilibrium condition. This results in a steady-state stoichiometry (δ^* in MAPbI$_{3+\delta^*}$, $\delta^* \propto [I_i'] + [I_i^\times] - [V_I^\bullet] - [V_I^\times]$) that differs from the equilibrium stoichiometry (δ_{eq} in MAPbI$_{3+\delta_{eq}}$). Importantly, we are ignoring any formation of higher order defects due to photogenerated electronic charges,[14] meaning that changes in ionic defect concentrations are expected under bias regardless of such events occurring. Note that such stoichiometry changes may correspond to compositions outside of

---

Table 2 Equations used to determine the non-equilibrium defect chemistry of MAPI, based on the reactions shown in Fig. 2 and Table 1

1. Electronic quasi-equilibrium	$G_{ext} = U_{rad} + U_{SRH} + U_{Aug} + U_I$
2. Electroneutrality	$[V_I^\bullet] + [h^\bullet] - [I_i'] - [e'] = 0$
3. Iodide interstitials quasi-equilibrium	$U_{\bar{F}} + \vec{R}_{n,i} - \overleftarrow{R}_{n,i} + \vec{R}_{p,i} - \overleftarrow{R}_{p,i} = 0$
4. Iodide vacancies quasi-equilibrium	$U_{\bar{F}} - \vec{R}_{n,v} + \overleftarrow{R}_{n,v} - \vec{R}_{p,v} + \overleftarrow{R}_{p,v} = 0$
5. Iodine interstitials quasi-equilibrium	$\vec{R}_{n,i} - \overleftarrow{R}_{n,i} + \vec{R}_{p,i} - \overleftarrow{R}_{p,i} - \vec{R}_{sg,i} + \overleftarrow{R}_{sg,i} = 0$
6. Iodine vacancies quasi-equilibrium	$-\vec{R}_{n,v} + \overleftarrow{R}_{n,v} - \vec{R}_{p,v} + \overleftarrow{R}_{p,v} + \vec{R}_{sg,v} - \overleftarrow{R}_{sg,v} = 0$

---

the material's stability region, an aspect that is not included here.[14]

We conclude that, if only one ionic defect is involved in redox reactions (here interstitials $I_i^\times/I_i'$, but similar results would be obtained for vacancies), the application of a light bias to the mixed conductor effects the following:

– The concentration of the neutral iodine defects $[I_i^\times]$ and $[V_I^\times]$ are exclusively determined and fixed by the value of $P(I_2)$, i.e. light-independent, based on the mass-action constants $K_{sg,i}$ and $K_{sg,v}$ in Table 1.

– The rate equations involving reactions (n,i) and (p,i), and the generation and recombination of electronic charge carriers determine the values of n, p and $[I_i']$.

– The value of $[V_I^\bullet]$ is fixed based solely on the value of $[I_i']$ according to the anti-Frenkel disorder reaction, which may shift but remains in equilibrium ($\Delta\mu_{\bar{F}} = 0$). This means that light can induce a change in stoichiometry in the mixed conductor with respect to the equilibrium condition.

Essentially, to obtain the data in Fig. 3, only eqn (1)–(3) in Table 2 need to be solved in combination with the mass-action laws for reactions $(\bar{F})$, (sg,i) and (sg,v). For all calculations in this section, we can obtain exact solutions to the problem by referring to the assumption that neutral defects remain in equilibrium with the gas phase, a condition that we refer to below as "sg-eq".

In Fig. 3b, we display the resulting graphs of QFLS as a function of $P(I_2)$ (red dotted line), as well as of the rates of recombination associated with the different mechanisms considered here. We find that U_{SRH} dominates for $P(I_2) \approx P(I_2)_i$, while U_{Aug} is dominant in the N and P regions (very high or very low $P(I_2)$). The QFLS is always lower than for the radiative limit (QFLS$_{rad}$) and it approaches such limit for two narrow ranges of $P(I_2)$. The position of the QFLS maxima corresponds to the situations where the contribution of R_{rad} to the total recombination is fractionally largest, and where $R_{SRH} = R_{Aug}$. Note that the latter condition is not general, but it is based on the input parameters used here ($\tau_n = \tau_p$, $n_1 = p_1$ and $\gamma_n = \gamma_p$). The local minimum observed for $n = p$ is consistent with the Shockley–Read–Hall theory of recombination (in the case of $\tau_n = \tau_p$ and for a mid-gap trap level). The slope of the QFLS vs. $\log_{10} P(I_2)$ can be evaluated as the sum of the slopes associated with electrons and holes in the Kröger–Vink diagram times a $k_B T \ln[10]$ factor. The data in Fig. 3b highlight that the QFLS obtained for a mixed conducting film (here MAPI) depends non-monotonically on the component partial pressure (here $P(I_2)$). Because QFLS is a proxy for the maximum open circuit potential which can be achieved once the material is embedded in a complete solar cell, this analysis emphasizes the importance of the component partial pressure for controlling the performance of optoelectronic devices based on mixed conductors.[41]

In Fig. 3c, we illustrate schematically the corresponding changes in electrochemical potentials for all defects where changes in both the ionic and electronic situations under bias (solid lines) are compared with the equilibrium solution (dashed lines). Consistently with the data in Fig. 3a, $\delta\tilde{\mu}_{V_I^\bullet} = -\delta\tilde{\mu}_{I_i'} = -\delta\tilde{\mu}_{I^-}$ ($\Delta\mu_{\bar{F}} = 0$) at any $P(I_2)$, with $\delta\tilde{\mu}_{V_I^\bullet} \approx 0$ in the
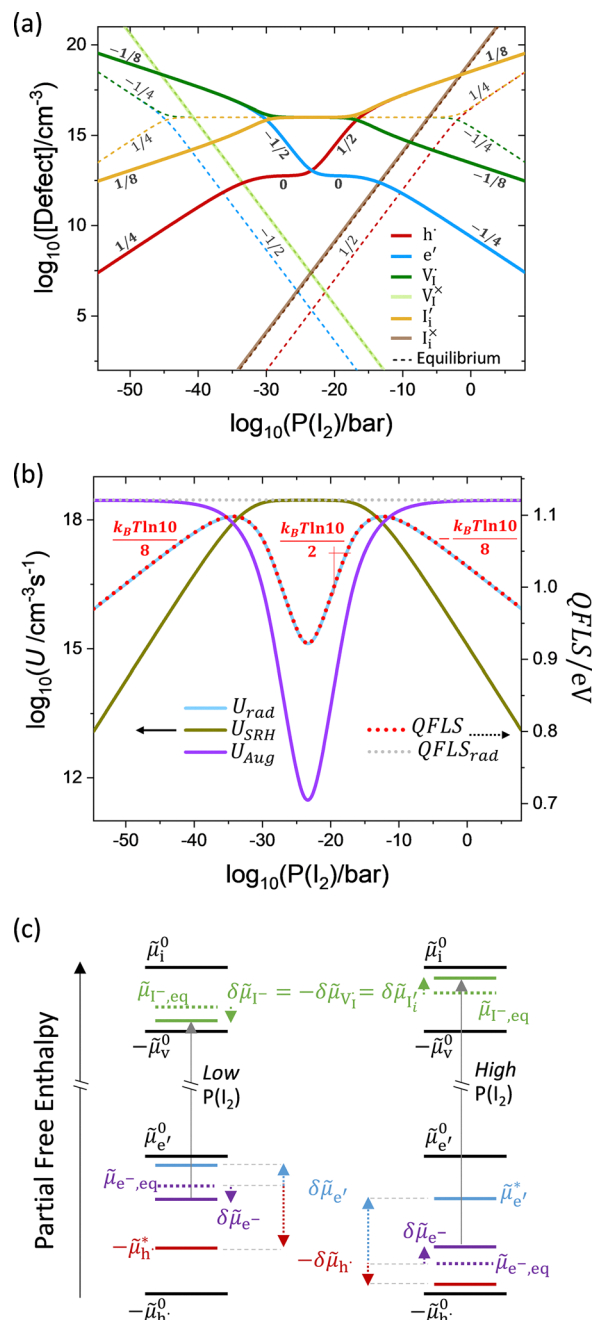

Fig. 3 Light-induced stoichiometry change in a mixed conductor with a single redox-active ionic defect. (a) Iodine partial pressure ($P(I_2)$) dependence of the steady-state electronic and ionic defect concentrations in MAPI at equilibrium and under light ($\sim10^{-3}$ suns) plotted in a Kröger–Vink diagram (the numbers close to the data refer to the corresponding slopes). The calculation refers to assuming the redox reaction occurring with iodine interstitials only, and $\Gamma_{I,i} = 1$. (b) Net recombination contributions and quasi-Fermi level splitting. (c) Schematic energy diagram emphasizing the change in the position of the electrochemical potentials with respect to the electronic and ionic standard potentials, going from equilibrium (dashed lines) to the situation under light (solid lines), and for cases of low and high $P(I_2)$.[8]

intrinsic region under light. Because the steady-state condition $\mu_{I,MAPI} = \frac{1}{2}\mu_{I_2,g}$ is valid both at equilibrium and under bias,

based on $\mu_{I,MAPI} = \tilde{\mu}_{I^-}^*, - \tilde{\mu}_{e^-}^*$, it follows that $\delta\tilde{\mu}_{I^-} = \delta\tilde{\mu}_{e^-}$ at any given $P(I_2)$. In Section 3 of the SI, we provide more details on the analysis of this quasi-equilibrium as well as the asymptotic trends for very low and very high $P(I_2)$.

The data in Fig. 3 refer to the case of $\Gamma_{p,i} = 10^{-2}$ (low hole trapping rate by I_i'). Combined with a balanced interaction of interstitials with electrons and holes ($\Gamma_{I,i} = 1$), this corresponds to a negligible contribution of recombination due to redox reactions with iodide interstitials U_I compared to other recombination pathways for the selected light intensity. In Fig. 4, we display the calculated defect concentrations and QFLS using the same input parameters as in Fig. 3, but with varying rates of hole trapping at iodine interstitials, parameterized through $\Gamma_{p,i}$. Simultaneous relative variations in electron trapping at iodide interstitials are ensured by selecting $\Gamma_{I,i} = 1$ in all cases. Fig. 4a indicates that, for large values of $\Gamma_{p,i}$, all defect concentrations are varied significantly from the situation shown in Fig. 3 in the high $P(I_2)$ region. The resulting QFLS (Fig. 4b) shows a significant drop in such region, which is ascribed to a dominant electron–hole recombination contribution mediated by the forward reactions associated with (n,i) and (p,i). Such contribution is compared with the total net recombination deriving from all the other mechanisms considered (inset of Fig. 4b).

We note that the Shockley–Read–Hall rate for recombination mediated by immobile traps is established based on the parameters n_1, p_1, which depend on the energetic position of the trap, and τ_n, τ_p, which depend on the (fixed) concentration and the capture coefficient of the trap. While the recombination due to redox reactions involving $I_i^\times/I_i'$ follows a similar principle, the concentration of such recombination centers is determined by the overall evaluation of the charge carrier quasi-equilibrium. In Fig. 4, U_I is dominant at high $P(I_2)$, due to the increase in $I_i^\times$ and I_i' defect concentrations. The dominant recombination mechanism for different $P(I_2)$ values is shown schematically in Fig. 4c (referring to the $\Gamma_{p,i} = 10^6$ case). The $I_i^\times/I_i'$ energy level is included within the energy bandgap.

Fig. 5a shows the influence of $\Gamma_{I,i}$ on the defect quasi-equilibrium. As the reaction (sg,i) is at equilibrium in this scenario, $\Gamma_{I,i}$ is a measure of the degree to which the "hole channel" vs. the "electron channel" control the iodine incorporation/excorporation at equilibrium (see Table 1 and Fig. 2). Changing $\Gamma_{I,i}$ does not vary the equilibrium defect concentrations (dashed lines in the Kröger–Vink diagrams) as these depend only on the mass-action constants. On the other hand, the position of the intrinsic region under light shifts on the $P(I_2)$ axis when varying $\Gamma_{I,i}$, while always remaining within the boundaries of the intrinsic region defined by the equilibrium case ($n \geq n_{eq}$ and $p \geq p_{eq}$). The iodine partial pressure $P(I_2)_i^*$ at which $n = p$ and $[V_I^\bullet] = [I_i']$ refers to the intrinsic condition under light. While $P(I_2)_i^*$ is essentially the same as $P(I_2)_i$ for the example in Fig. 3 ($\Gamma_{I,i} = 1$ and low $\Gamma_{p,i}$), Fig. 5a shows that, in general, $P(I_2)_i^* \neq P(I_2)_i$.

Fig. 5b highlights the shrinking of the intrinsic region with increasing light intensity (the same input parameters as for Fig. 3 are used). The trends in QFLS resulting from varying $\Gamma_{I,i}$ or light intensity are shown in Fig. 5c, emphasizing that the
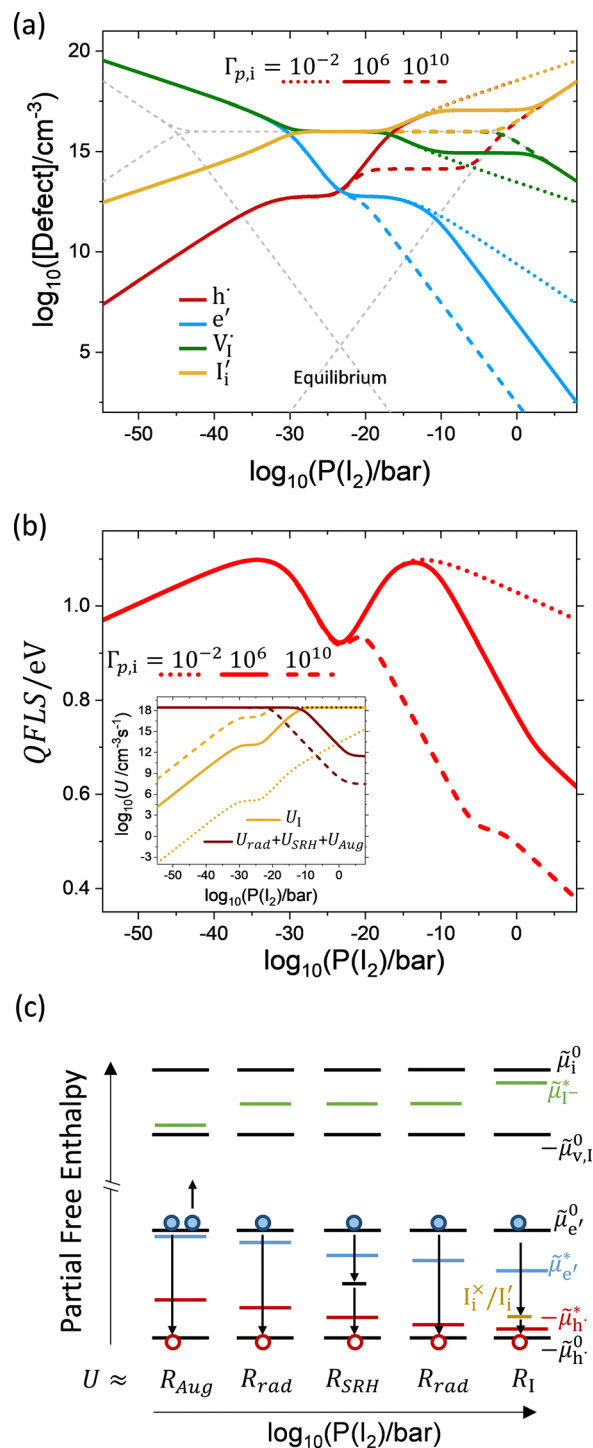
(a)

(b)

(c)

Fig. 4 Light-induced stoichiometry changes in a mixed conductor with a single redox-active ionic defect, which also contributes significantly to electron–hole recombination. (a) Defect concentration and (b) QFLS for a MAPI film calculated for $\Gamma_{p,i} = 10^{-2}$, 10^6 and 10^{10} (corresponding to $\vec{k}_{p,i}^\bullet = 2.1 \times 10^{-24}$, 2.1×10^{-16} and 2.1×10^{-12} cm^3 s^{-1}). The inset in (b) shows the comparison between the combined recombination contribution from radiative, SRH and Auger mechanisms, and the contribution U_I due to the redox reactions (n,i) and (p,i). Illumination of 10^{-3} suns and $\Gamma_{I,i} = 1$ are considered. (c) Generalized energy diagram showing the dominant recombination mechanisms for different $P(I_2)$ regions in (a) and (b) ($\Gamma_{p,i} = 10^6$ case). The $I_i^\times/I_i'$ energy level is included (~ 0.3 eV above the valence band maximum based on input parameters).
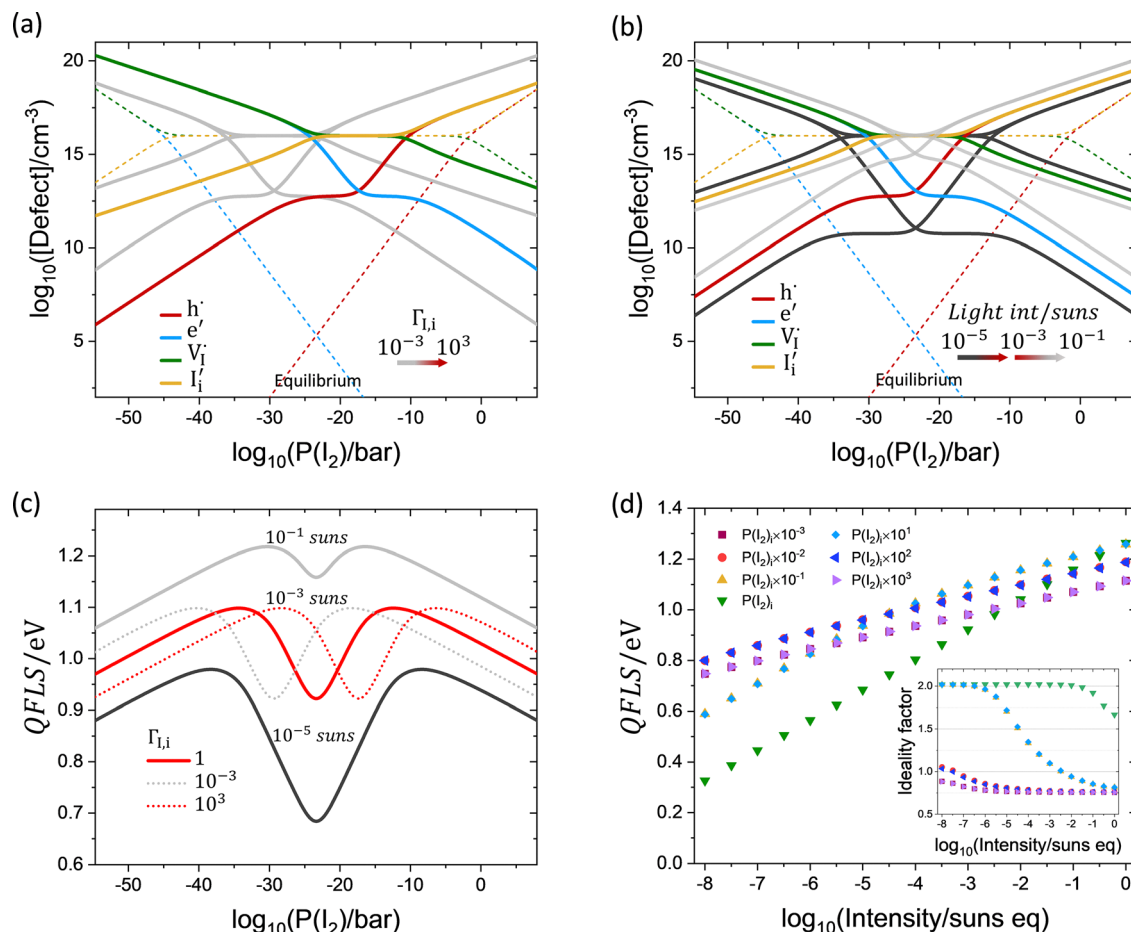
Fig. 5 Variations in the defect chemical quasi-equilibrium of the illuminated mixed conductor due to changes in electronic and ionic properties, as well as in the light intensity. Calculated defect concentrations *vs.* $P(I_2)$ in MAPI (a) under $\sim 10^{-3}$ suns equivalent illumination comparing situations where $\Gamma_{I,i} = 10^{-3}$ or $\Gamma_{I,i} = 10^{3}$ and (b) for $\Gamma_{I,i} = 1$ for varying bias light intensities ($\Gamma_{p,i} = 10^{-2}$ in all cases). The corresponding QFLS profiles for the data in (a) and (b) are shown in (c). (d) Ideality factor analysis obtained from the light intensity dependent calculations of the QFLS.

$P(I_2)$ values corresponding to local QFLS maxima are dependent on such parameters. The situation is further complicated if larger values of $\Gamma_{p,i}$ are considered (in Fig. 5, $\Gamma_{p,i} = 10^{-2}$). Fig. 5d displays the light intensity dependence of QFLS evaluated at different values of $P(I_2)$ for $\Gamma_{I,i} = 1$. The data once again illustrate the influence of $P(I_2)$ on the dominant recombination mechanism, as also highlighted by the trends in local ideality factor (defined here as $\frac{1}{k_B T}\frac{d(QFLS)}{d\ln(\text{Intensity})}$, see inset).

To conclude this section, we discuss a simple example to understand possible implications of the model under realistic experimental conditions. Let us consider a MAPI film equilibrated at $P(I_2)_i$. We hypothesize that only interstitials are redox active and that $\Gamma_{I,i} \gg 1$ (*e.g.* see Fig. 5a for the case of $\Gamma_{I,i} = 10^{3}$, colored lines). The interstitial redox reaction mediated by holes essentially dominates in a wide range of $P(I_2)$, where the definition of the (pseudo)mass action constant $K_{p,i}$ (see Table 1) can be extended to the situation under light. We can then write for the iodine quasi-chemical potential associated with holes $\mu^*_{I,p} = \mu_{I,MAPI} = \frac{1}{2}\mu_{I_2,g}$, also implying $\delta\tilde{\mu}_{I^-} = -\delta\tilde{\mu}_p$. The latter relationship means that, upon the increase of the hole

concentration in the mixed conductor (assuming $p \ll [V_I^\bullet]$ and $p \ll [I_i']$) due to illumination, a fractionally equivalent increase in $[V_I^\bullet]$ and decrease in $[I_i']$ is expected (light-induced shift in stoichiometry and excorporation of iodine[14]). Importantly, when considering the condition of electroneutrality in the bulk of the material, we find that there is a limit to the increase in $[V_I^\bullet]$ to as far as the combination of its charge compensating defects, that is $[V_I^\bullet] \approx n + [I_i']$.

We also note that, for the same mixed conductor equilibrated at high $P(I_2)$, illumination can lead to a shift in stoichiometry of opposite sign (incorporation of iodine, decrease in $[V_I^\bullet]$ and increase in $[I_i']$) due to the condition of electroneutrality $p \approx [I_i']$. The effect naturally fades towards a zero change in ionic defect concentrations under light only for the asymptotic case of $\Gamma_{I,i} \to \infty$, for which $\delta\tilde{\mu}_{I^-} = -\delta\tilde{\mu}_p$ is valid at any $P(I_2)$ (see also Scheme S1 in the SI).

Multiple redox-active mobile ionic defects: ionic disorder out of equilibrium

We now consider situation (b) in the model shown in Fig. 2, whereby both interstitial and vacancy defects interact with

electronic charge carriers *via* redox reactions. For now, we shall continue to assume the "sg-eq" condition. Such a situation may be relevant only to very small particles of the mixed conductor (although see discussion below).

Fig. S2 shows that if both interstitials and vacancies show similar coupling to electrons and to holes ($\Gamma_{I,i} = \Gamma_{I,v}$) and the recombination mediated by the mobile ions is negligible (low $\Gamma_{p,i}$ and $\Gamma_{n,v}$), essentially unchanged trends are found compared with the results obtained using a single redox-active ion (Fig. 3 and 5). If either of these conditions are not met, different trends from the single redox active mobile defect case are obtained (see Fig. S3 for $\Gamma_{I,i} \neq \Gamma_{I,v}$ and low $\Gamma_{p,i}$, $\Gamma_{n,v}$, and Fig. S4 for the case of high $\Gamma_{p,i}$, $\Gamma_{n,v}$ and $\Gamma_{I,i} = \Gamma_{I,v}$). Despite such deviations, equilibrium in the ionic disorder is maintained under light, although shifted with respect to the dark equilibrium case (*i.e.* light induces stoichiometry changes in the mixed conductor).

We now discuss the implications of both above conditions not being met. Fig. 6 explores the effect of the parameters $\Gamma_{I,i}$ and $\Gamma_{I,v}$, which define to what extent the $I_i^\times/I_i'$ and the $V_I^\times/V_I^\bullet$ quasi-equilibria are established by reactions with holes ($\Gamma_I \gg 1$) or electrons ($\Gamma_I \ll 1$). The data are obtained considering a value of $\Gamma_{p,i} = \Gamma_{n,v}$ as large as 10^{11}.

Fig. 6a is the reference situation where the redox reactions involving interstitials and the ones involving vacancies are driven by electrons and holes to a similar extent ($\Gamma_{I,i} = \Gamma_{I,v}$), as discussed above for Fig. S4. As $\Gamma_{I,i} = \Gamma_{I,v} = 1$ (and $\Gamma_{p,i} = \Gamma_{n,v}$), the defect diagram preserves "symmetry" about the pressure value $P(I_2)_i$. The ionic defect profiles under light largely follow the same trends in the equilibrium and in the light biased cases. This contrasts with the results in Fig. 3, where significant changes in ionic defect concentrations are encountered especially in the high and low $P(I_2)$ ranges. Due to the large values of the redox reactions' rate constants (related to $\Gamma_{p,i}$ and $\Gamma_{n,v}$), the iodide vacancy reduction reaction (n,v) at low $P(I_2)$ and the iodide interstitial oxidation (p,i) at high $P(I_2)$ are essentially operating at equilibrium. Along with the sg-eq condition, this ensures minimal deviations from the equilibrium trends of the relevant defects in these two pressure ranges. The same occurs also for intermediate values of $P(I_2)$, due to the symmetrical interaction of the electronic carriers with the ionic defects.

Fig. 6b and c consider situations where the relevance of electrons and holes in the determination of the redox reaction quasi-equilibrium, as expressed by the parameters $\Gamma_{I,i}$ and $\Gamma_{I,v}$, is not the same for interstitials and vacancies ($\Gamma_{I,i} \neq \Gamma_{I,v}$). The data show a striking increase or decrease (Fig. 6b and c, respectively) in the concentration of both iodide vacancies and iodide interstitials under light with respect to equilibrium. Such observation implies that, for a mixed conductor with more than one type of redox-active ionic species, light can be used to increase or reduce the concentration of such ionic defects.

Such effect requires a deviation from the anti-Frenkel equilibrium due to illumination, which can be explained as follows. Increase in n tends to increase $[I_i']$ but decrease $[V_I^\bullet]$, while an increase in p has the opposite effect (see Table 1). Since $[I_i^\times]$
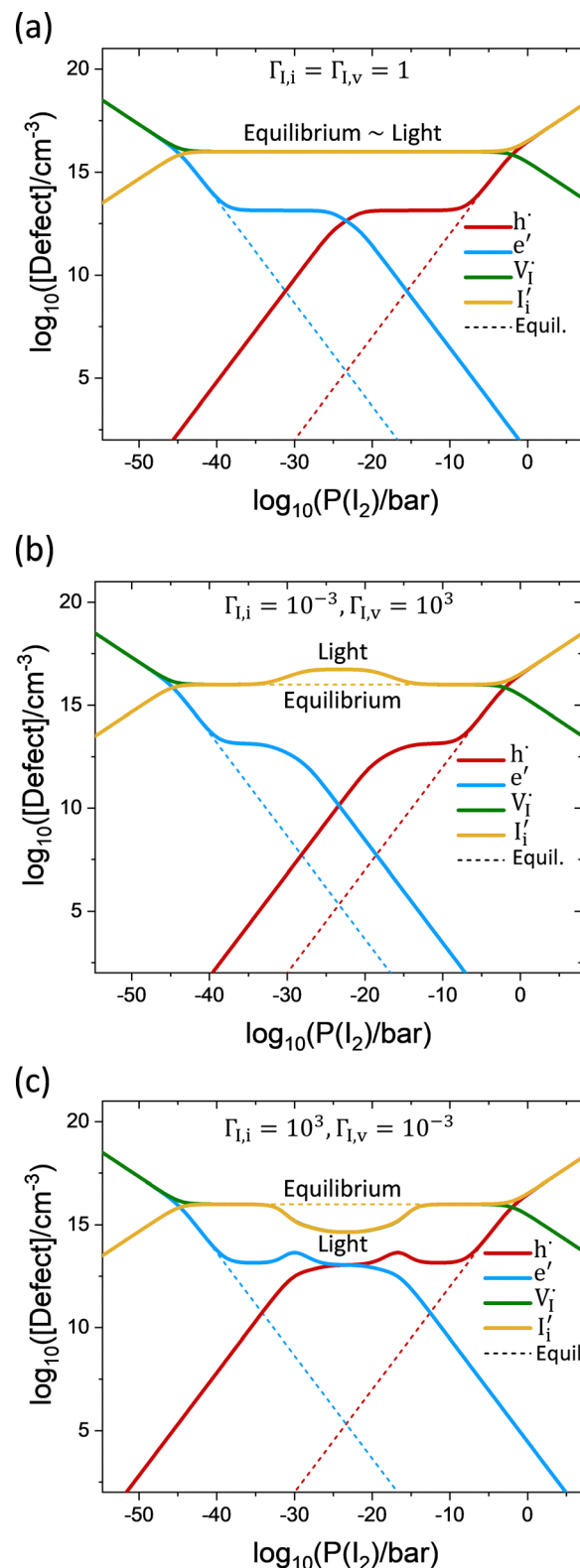

Fig. 6 Light-induced concentration increase or decrease of both redox-active ionic defects in a mixed conductor. The Kröger–Vink diagrams refer to a mixed conductor (MAPI) at equilibrium and under light (10^{-3} sun equivalent illumination), for situations where both iodide vacancies and interstitials participate in redox reactions with electrons or holes. Different values of the parameters $\Gamma_{I,i}$ and $\Gamma_{I,v}$ are used ($\Gamma_{p,i} = \Gamma_{n,v} = 10^{11}$ in all cases). (a) $\Gamma_{I,i} = \Gamma_{I,v} = 1$; (b) $\Gamma_{I,i} = 10^{-3}$ and $\Gamma_{I,v} = 10^3$; (c) $\Gamma_{I,i} = 10^3$ and $\Gamma_{I,v} = 10^{-3}$.

and $\left[V_I^\times\right]$ are fixed at any given $P(I_2)$, changes in the value of $\left[I_i'\right]$ and $\left[V_I^\bullet\right]$ depend on the rates of the reactions that "connect" each of them to either electrons or holes. Such connection is parameterized through $\Gamma_{I,i}$ and $\Gamma_{I,v}$.

For example, let us consider a MAPI film equilibrated at $P(I_2)_i$ and assume that holes dominate the redox chemistry of interstitials while electrons dominate the redox reactions involving vacancies ($\Gamma_{I,i} \gg 1$ and $\Gamma_{I,v} \ll 1$). As the equilibria expressed by the (pseudo)mass action constant $K_{p,i}$ and $K_{n,v}$ would tend to remain valid under light too (see Table 1 and Scheme S1 in the SI), their expression points to the reduction in both $\left[V_I^\bullet\right]$ and $\left[I_i'\right]$ at a fixed $P(I_2)$ (and therefore fixed $\left[I_i^\times\right]$ and $\left[V_I^\times\right]$ based on sg-eq).

Analytically, it is useful to define the parameter

$$
\begin{aligned}
X_{vi} &= \left(\overleftarrow{R}_{n,i} - \overrightarrow{R}_{n,i}\right) - \left(\overrightarrow{R}_{p,i} - \overleftarrow{R}_{p,i}\right) \\
&= \left(\overrightarrow{R}_{p,v} - \overleftarrow{R}_{p,v}\right) - \left(\overleftarrow{R}_{n,v} - \overrightarrow{R}_{n,v}\right).
\end{aligned}
\tag{13}
$$

The absolute value of X_{vi} corresponds to the absolute value of the electron–hole net recombination contribution involving two ionic defects. This can correspond to a positive net recombination where two ionic defects mediate the separate trapping of electrons and holes. It can also refer to a positive net thermal generation where the two defects mediate the separate de-trapping of electrons and holes.

If only one redox active defect is considered, $X_{vi} = 0$ by definition, at steady-state. If instead both interstitials and vacancies are redox active, as shown in Fig. 6, such condition is no longer necessarily true. Specifically, if $X_{vi} = 0$, the rate of electron trapping by each of the iodide vacancies or iodine interstitials is counter-balanced by an equal rate of hole trapping interacting with the same type of defect (this is the case when $\Gamma_{I,i} = \Gamma_{I,v}$). That means that no reaction between ionic defects is required to mediate the recombination (or thermal generation process).

If instead $X_{vi} \neq 0$, the fraction of the total electron–hole net recombination which is mediated by separate (de-)trapping of electronic charges by the two ionic defects also requires reaction between such ionic defects. Specifically, in the steady-state, such an electron–hole recombination process involves the recombination of the two ionic defects with the trapped carriers and the generation of the two original defects before trapping (similar argument applies to electron–hole thermal generation). The effective ionic defect generation term for charged anti-Frenkel pairs ($G_{\bar{F}}$) and neutral anti-Frenkel pairs ($G_{\bar{F}\times}$) are defined and, in steady-state, they relate to each other and to the X_{vi} term as follows:

$$
G_{\bar{F}} = -G_{\bar{F}\times} = X_{vi}
\tag{14}
$$

Importantly, and in contrast with the electronic generation term G_{ext}, these effective ionic defect generation terms can be positive or negative. This leads to the prediction that illumination can increase the concentration of ionic defects *via* a $G_{\bar{F}} > 0$ (analogously to the effect of a positive G_{ext} on the electronic charge carrier concentrations) but also decrease the concentration of ionic defects *via* a $G_{\bar{F}} < 0$. Based on eqn (10), (13) and

(14), we find that the rate eqn (3)–(6) in Table 2 related to the ionic defects represent different extended forms of the equations $G_{\bar{F}} = U_{\bar{F}}$ and $G_{\bar{F}\times} = U_{\bar{F}\times}$, respectively.

Based on this interpretation, the trends in Fig. 6 can be explained. By considering the parameter $h_{ion} = \log_{10}(\Gamma_{I,v}/\Gamma_{I,i})$, we found that situations where $G_{\bar{F}} = 0$, $G_{\bar{F}} > 0$ or $G_{\bar{F}} < 0$ refer to $h_{ion} = 0$, $h_{ion} > 0$ and $h_{ion} < 0$, respectively (see Fig. 6a–c, and analytical treatment in Section 2 of the SI relating $\Gamma_{I,v}$, $\Gamma_{I,i}$ and h_{ion} to SRH trapping parameters associated with the mobile ions).

We note that a similar change in concentration compared with the equilibrium case affects both ionic defects in the intrinsic regions of Fig. 6b and c. The resulting change in stoichiometry between the dark and the light-bias cases is therefore less significant here than for the situation displayed in the N and P regions of Fig. 3a. The latter largely reflects the discussion of previous studies on light-effects in halide and oxide perovskites (see introduction). On the other hand, obtaining simultaneous increase or decrease in the concentration of both ionic defects involved in the dominant ionic disorder reaction through light may open new opportunities in material science and beyond (see also next section).

Importantly, the data in Fig. 6 are obtained by considering the sg-eq condition, which is not necessarily valid for the multiple redox-active ionic defect case (Fig. 2b). This means that the concentration profiles for the neutral defects are assumed to be unperturbed under light compared with the equilibrium situation (see Fig. 3a), and that only the concentration of the anti-Frenkel pairs is subject to variations, which depend on the value of $\Gamma_{I,i}$, $\Gamma_{I,v}$ and $\Gamma_{p,i}$, $\Gamma_{n,v}$. When solving the full kinetic model which includes a finite rate for the solid–gas exchange reactions (sg-eq condition no longer valid), we found that both the charged and the neutral ionic defect concentrations are perturbed by light. The effect described above, with either an increase or a decrease of both $\left[I_i'\right]$ and $\left[V_I^\bullet\right]$, still occurs but to a lesser extent (see Section 5 of the SI).

Here, we discuss solutions under the sg-eq condition further, as these describe the upper limit to the anti-Frenkel nonequilibrium induced by illumination of the mixed-conductor. In Fig. 7a, the $\Delta\mu_{\bar{F}}$ and the QFLS profiles corresponding to the data in Fig. 6 are illustrated. The conditions that lead to an enhancement in the ionic concentrations also lead to a drop in QFLS, while an increase in QFLS is observed when redox reactions reduce the mobile ion concentrations. This can be explained since U_I scales with the concentration of mobile ions that can mediate recombination. In Fig. 7b, the electronic generation rate as well as the anti-Frenkel pair effective generation rate are shown. Consistent with the definition of the effective ionic defect generation rate, $|G_{\bar{F}}| \leq G_{ext}$. Fig. 7c shows a schematic including the extended energy level diagram summarizing these findings. In the SI, we show other examples where the condition $\Gamma_{I,i} \neq \Gamma_{I,v}$ ($h_{ion} \neq 0$) results in $\Delta\mu_{\bar{F}} \neq 0$, including the case where the same electronic charge carrier dominates redox reactions with both interstitials and vacancies (see Fig. S6).

Fig. 8 illustrates the dependence of the ionic defect concentration enhancement or depression on the parameters $\Gamma_{I,i}$, $\Gamma_{I,v}$, and $\Gamma_{p,i}$, $\Gamma_{n,v}$, based on the trends in $\Delta\mu_{\bar{F}}$. While the sign as well
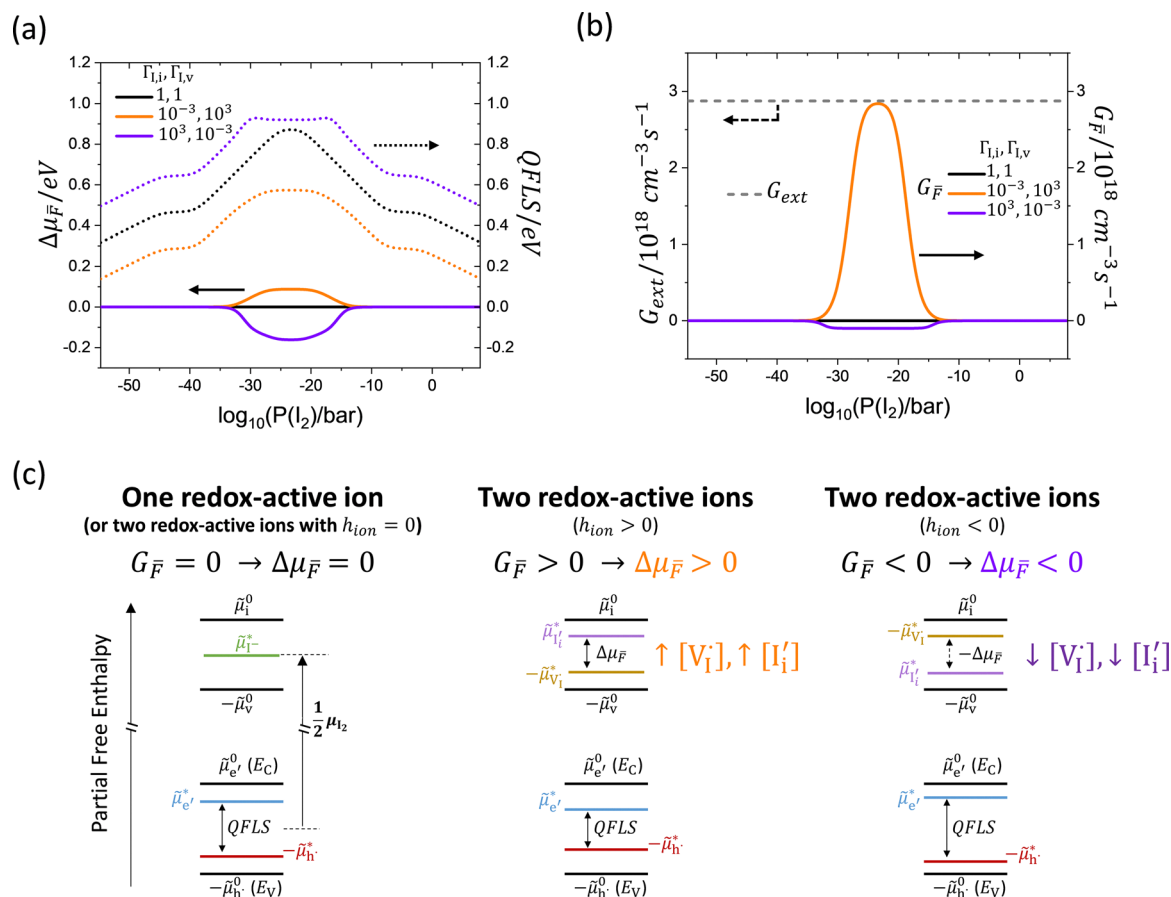
Fig. 7 Introducing the ionic defect pair chemical potential in analogy to the electronic chemical potential to describe quasi-equilibrium in the mixed conductor under illumination. The consequences of including two redox-active mobile ionic defects in the defect chemical quasi-equilibrium of a mixed conductor exposed to light, assuming equilibrium of the neutral defects ($I_i^\times$ and $V_I^\times$) with the gas phase (sg-eq) are displayed referring to (a) the ionic ($\Delta\mu_{\bar{F}}$) and the electronic (QFLS) chemical potentials. (b) Electronic generation rate G_{ext} used in the calculations (10^{-3} suns equivalents) and resulting effective anti-Frenkel ionic generation rate $G_{\bar{F}}$ for the three situations considered in (a) and in Fig. 6. (c) Generalized energy level diagram corresponding to the (left) unchanged, (center) increased and (right) decreased charged ionic defect concentration upon illumination.

as the magnitude of $\Delta\mu_{\bar{F}}$ depend on h_{ion}, the data show that obtaining perceptible deviations from the anti-Frenkel equilibrium requires a sufficiently large value of both $\Gamma_{p,i}$ and $\Gamma_{n,v}$. This is because the extent of the non-equilibrium in the anti-Frenkel disorder (magnitude of $\Delta\mu_{\bar{F}}$) correlates with the fraction of the overall electron–hole recombination rate that is due to mobile-ion mediated reactions (dictated by $\Gamma_{p,i}$, $\Gamma_{n,v}$ as well as by $\Gamma_{I,i}$, $\Gamma_{I,v}$). Fig. 8a shows that, as the concentration of ionic defects increases for very large values of h_{ion} and $\Gamma_{p,i} = \Gamma_{n,v} = 10^{11}$, $\Delta\mu_{\bar{F}} \approx$ QFLS (see also pseudo-mass action laws in Table 1 and Scheme S1 in the SI).

Fig. 8b and d highlight that, for increasing $\Gamma_{p,i}$ and $\Gamma_{n,v}$, the QFLS decreases less substantially if $h_{ion} < 0$ than if $h_{ion} > 0$. This is due to the depression, rather than enhancement, in $[I_i']$ and $[V_I^\bullet]$, which mediate recombination. In other words, light can induce enhancement or reduction in the concentration of recombination-active ionic defects. In either case, it significantly influences not only the ionic but also the electronic quasi-equilibrium. Section 7 of the SI shows similar calculations performed without the SRH recombination mediated by

immobile defects to highlight the effect of minimizing the recombination due to anti-Frenkel pairs (for $h_{ion} < 0$) on the QFLS. We emphasize that such situations cannot improve the value of QFLS beyond the limit where the anti-Frenkel defects are not recombination active (see Fig. S7 and S8).

Summary and outlook

In summary, the analysis presented in this work:

– provides a framework for the study of redox reactions, electron–hole recombination and solid–gas component exchange reactions when photoactive mixed conducting materials are illuminated

– outlines guidelines for material design where ionic defect concentrations (trap densities) can be increased and, strikingly, also decreased by light

– proposes a rationale for the development of photoelectrochemical systems that allow for stoichiometry control using optical stimuli
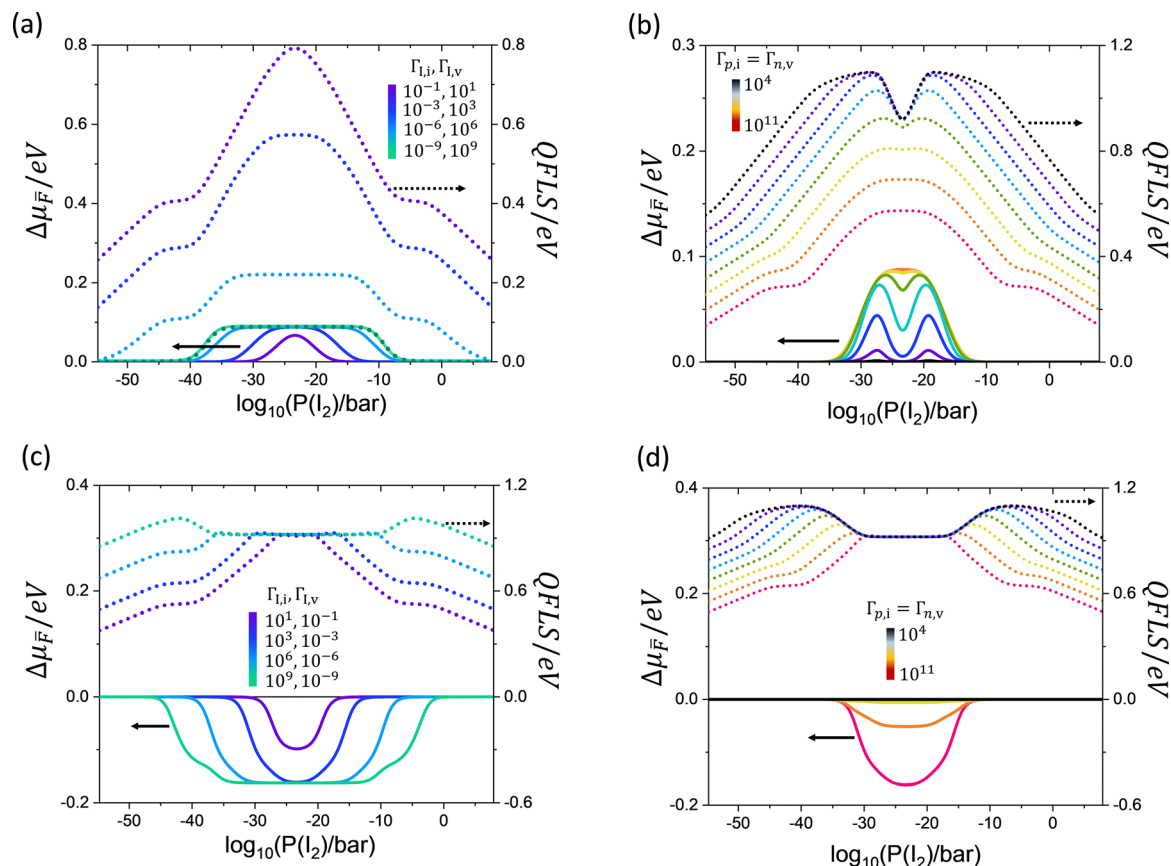
Fig. 8 Dependence of the ionic ($\Delta\mu_{\bar{F}}$) and electronic (QFLS) change in chemical potential on the $\Gamma_{I,i}$, $\Gamma_{I,v}$, and $\Gamma_{p,i}$, $\Gamma_{n,v}$ parameters, as a function of $P(I_2)$. Trends for (a) increasing $h_{ion} > 0$ ($\Gamma_{p,i} = \Gamma_{n,v} = 10^{11}$), (b) increasing $\Gamma_{p,i} = \Gamma_{n,v}$ ($\Gamma_{I,i} = 10^{-3}$, $\Gamma_{I,v} = 10^{3}$), (c) decreasing $h_{ion} < 0$ ($\Gamma_{p,i} = \Gamma_{n,v} = 10^{11}$), and (d) increasing $\Gamma_{p,i} = \Gamma_{n,v}$ ($\Gamma_{I,i} = 10^{3}$, $\Gamma_{I,v} = 10^{-3}$). All remaining parameters are the same as the ones used in Fig. 3. $h_{ion} = \log_{10}\left(\dfrac{\Gamma_{I,v}}{\Gamma_{I,i}}\right)$.

– emphasizes the importance of understanding electronic and ionic kinetic properties, especially in the context of solar energy conversion devices based on mixed conductors where mobile ions provide a significant contribution to the total electron–hole recombination rate.

– has direct implications to the field of halide perovskites, as well as to any situation where a mixed conducting system is exposed to light (or voltage) bias

This study presents the fundamental effect that light has on the steady-state ionic and electronic bulk properties of mixed conductors. The model can be extended to include transport and interfacial effects, and it can be integrated in physical models of complete mixed conducting devices for the study of their steady-state as well as transient response when exposed to light and/or voltage bias.[20,29,42–46]

In view of a more complete analysis in one dimension, where the continuity equations referring to mobile defects also include transport terms, we anticipate that:

– The assumption of uniform optoelectronic excitation within the mixed conductor used here would hold only for films that are significantly thinner than the absorption length of the material for the specific excitation wavelength used.

– For thick films, nonequilibrium due to illumination may extend over longer distances than the absorption length in the case of compounds that show long electronic diffusion lengths (as is the case for halide perovskites[47]). At locations that are sufficiently far from the illuminated surface (distance » diffusion and absorption lengths), the equilibrium defect concentrations at the specific component partial pressure used are maintained (note that diffusion and absorption lengths may depend on the component partial pressure).

– Accounting for ionic defects forming specifically at the surface (and at interfaces) may be critical to accurately describe solid–gas (solid–solid, solid–liquid) exchange as well as interfacial space charge effects. Additional terms associated with surface electronic recombination mediated by such defects can be a dominant loss mechanism in mixed conductors with long bulk charge carrier lifetimes.

– Finite rates of ionic transport and stoichiometric polarization within macroscopic systems, as well as slow solid–gas component exchange reactions may all play a role, depending on the operating conditions, as the rate determining step to reaching quasi-equilibrium. These factors influence the extent of the position-dependent nonequilibrium obtained for the steady-state situation, for which this model represents an upper

limit (see Section 5 of the SI in the context of solid–gas exchange kinetics).

– At steady-state under illumination, no net mass transport within the sample and no net mass exchange at the solid–gas phase are expected. For cases where the ionic disorder reaction shifts but remains at equilibrium under light (*e.g.* case (a) in Fig. 2, one redox active defect), any gradient in chemical potential of the ionic defects across the film's depth must be counterbalanced by an electrostatic potential term (space charge). This ensures a constant $\tilde{\mu}_{1^-}^*$ and zero current for each of the ionic defects at all positions. On the other hand, nonequilibrium in the ionic disorder reactions (*e.g.* case (b) in Fig. 2, two redox active defects) may be reflected in nonzero steady-state transport terms for ionic defects within the sample. Equal and opposite ionic current terms for iodide vacancies and interstitials result in net zero mass transport, similarly to the nonzero steady-state electron and hole current expected in such systems.

Additional extensions considering the full ionic defect chemical treatment in terms of ion type and range of accessible oxidation states,[34,40] as well as further pathways to ionic defect formation and association could be subject of future work. The current model also represents a starting point for the investigation of photo-induced phase-instability and degradation effects, important questions for the application of halide perovskites.[14,37,48,49]

Finally, we comment on possible experiments that could test and validate the effects predicted by the model in sections a and b of the Results and discussion.

(a) Previous observations of light-induced ionic responses in MAPI and STO are consistent with the general framework discussed in section a, concerning light-induced component exchange (iodine and oxygen, respectively) and stoichiometry changes in the mixed conductor.[14,19,22–24,50,51] The study of similar light effects in other mixed conductors, where interactions between ionic defects and electronic charges can be controlled, should be the subject of future studies. Importantly, estimating changes in mobile ionic defect concentrations from electrochemical measurements of partial conductivities using the analysis typically applied to systems at equilibrium may not always be possible, due to additional coupling between the ionic and electronic response (*e.g.* ionic-to-electronic current amplification[15,46,52,53]). The use of multiple independent techniques that can also quantify component incorporation/excorporation can provide more direct evidence for such effects,[14] provided that the experimental method's sensitivity and the material's phase stability allow for reliable analysis.

(b) The enhancement/reduction of both ionic defects' concentration in a mixed conductor exposed to light has, to our knowledge, not been discussed before. Modulation of transport and lifetime of electronic charge carriers upon photo-induced decrease or increase in the concentration of both ionic defects is one of the exciting perspectives for such a prediction. Probing such changes in combination with a negligible variation in stoichiometry may provide compelling, yet indirect, evidence of the effect. Direct quantification of ionic

defect concentrations could be achieved *via* spectroscopic techniques or from the analysis of structural measurements on specifically designed materials providing clear probes for such quantities. Finally, the design of photoelectrochemical devices including electrodes with opposite selectivity to the two ionic defects would allow the measurement of photoinduced ionic currents and electrochemical potentials, in analogy to the measurement of a traditional solar cell (see also demonstrations of water based protonic solar cells[54,55]). Such approach represents both a promising strategy to investigate light-induced ionic effects in mixed conductors as well as an exciting direction in the development of novel systems for energy conversion and storage, sensing, and computing applications.

Conclusions

We present a model that describes the effect of light on the ionic and electronic properties of a mixed ionic–electronic conductor. Using a simplified description of the halide perovskite methylammonium lead iodide (MAPI) as a model system, we obtain and explore trends that are relevant to any photoactive mixed conductor under fixed component partial pressure. We focus on the rate equations describing defect reactions and neglect defect transport to the solid–gas interface. By coupling the ionic (anti-Frenkel) disorder reaction, the iodine redox reactions and exchange with the gas phase with the electronic (photo-)generation and recombination, we predict the trends of ionic and electronic defect concentrations as a function of the component partial pressure (for MAPI this refers to iodine). We discuss the material's thermodynamic and kinetic parameters that control the steady-state solution to such problem, with a particular focus on the relative contribution of the two electronic charge carriers to the redox and solid–gas exchange reactions. Knowledge of such aspects allows one to determine the steady-state quasi-Fermi level splitting in the material, with relevance to the optimization of solar cells. Light induces changes in stoichiometry (the equilibrium in the ionic disorder reaction is maintained and only shifted) if a single ionic defect is redox-active, regardless of the solid–gas exchange kinetics. As a result, illumination can lead to significant changes in the concentration of mobile ionic defects compared with the dark case. Including redox reactions for multiple ionic defects (for example iodide vacancies and interstitials in MAPI) opens the possibility of taking the ionic disorder reaction out-of-equilibrium. This points to the intriguing opportunity of designing systems where defect concentrations are increased or decreased by light ("light-driven ionic defect generation or recombination"). Such scenarios are described by introducing an ionic defect pair chemical potential and an effective ionic defect generation rate, both of which can be positive (in analogy to their electronic counter parts) but also negative, depending on the ionic–electronic interactions.

Conflicts of interest

There are no conflicts to declare.

List of symbols

Symbol	Meaning, units
e', $h^{\bullet}$, I_i', $V_I^{\bullet}$, $I_i^{\times}$, $V_i^{\times}$	Point defect notation for electrons, holes, iodide interstitials, iodide vacancies, iodine interstitials, iodine vacancies, —
n, p, $[I_i']$, $[V_I^{\bullet}]$, $[I_i^{\times}]$, $[V_i^{\times}]$	Concentration of electrons, holes, iodide interstitials, iodide vacancies, iodine interstitials, iodine vacancies, cm^{-3}
I_2, g	Iodine molecule in the gas phase, —
$P(I_2)(P(I_2)_i)$	Iodine partial pressure (at the intrinsic condition), bar
$\mu_j(\tilde{\mu}_j)$ $j = n, p, \ldots$	Equilibrium (electro)chemical potential of species j, eV
$\mu_j^*(\tilde{\mu}_j^*)$	Nonequilibrium (electro)chemical potential of species j, eV
$\delta\mu_j(\delta\tilde{\mu}_j)$	Deviation from equilibrium in the (electro)chemical potential of species j, eV
$\vec{R}_r$, $\overleftarrow{R}_r$ $r = \bar{F}^{\times}\bar{F}$, sg, i, sg, v $\ldots$	Forward and backward rates for reaction r (see Table 2), cm^{-3} s^{-1}
$\vec{k}_r$, $\overleftarrow{k}_r$	Forward and backward rate constants for reaction r (see Table 2), s^{-1}, cm^{-3} s^{-1}, cm^{-6} $s^{-1} \ldots$ depending on r
K_r	Mass action constant of reaction r (see Table 2), Depends on r
R	Electron–hole recombination rate, cm^{-3} s^{-1}
G_{ext}	Electron–hole generation rate due to external illumination, cm^{-3} s^{-1}
U_k k = rad, SRH, Aug, I	Electron–hole net recombination due to the process k (radiative, Shockley-Read-Hall, Auger, iodine defect mediated), cm^{-3} s^{-1}
$\Gamma_{p,i}$	Normalized equilibrium hole trapping rate by I_i' at $P(I_2)_i$, —
$\Gamma_{n,v}$	Normalized equilibrium electron trapping rate by $V_I^{\bullet}$ at $P(I_2)_i$, —
$\Gamma_{I,i}$	Ratio between the rate of I_i' oxidation by holes and the rate of electron release from I_i' at equilibrium and at $P(I_2)_i$, —
$\Gamma_{I,v}$	Ratio between the rate of $V_I^{\times}$ oxidation by holes and the rate of electron release from $V_I^{\times}$ at equilibrium and at $P(I_2)_i$, —
h_{ion}	$\log_{10}(\Gamma_{I,v}/\Gamma_{I,i})$, —
$G_{\bar{F}}(G_{\bar{F}^{\times}})$	Effective generation rate of (neutral) anti-Frenkel defects, cm^{-3} s^{-1}
X_{vi}	Absolute value of electron–hole net recombination involving generation/recombination of a vacancy–interstitial pair, cm^{-3} s^{-1}
$U_{\bar{F}}(U_{\bar{F}^{\times}})$	Net recombination of (neutral) anti-Frenkel defects, cm^{-3} s^{-1}
QFLS	Quasi-Fermi level splitting (i.e. electron–hole chemical potential), eV
$\Delta\mu_{\bar{F}}$	Anti-Frenkel ionic defect pair chemical potential, eV

Data availability

The data in this work are available at **https://doi.org/10.5281/zenodo.16928557**. The codes used to generate the data are available at **https://github.com/d-moia/MIEC_light**.

Supplementary information (SI) is available. See DOI: **https://doi.org/10.1039/d5mh01231g**.

Acknowledgements

References

1 J. Maier, *Physical Chemistry of Ionic Materials*, Wiley-VCH Verlag GmbH & Co. KGaA, 2nd edn, 2023.

2 S. M. Sze and K. N. Kwok, *Physics of Semiconductor Devices Physics of Semiconductor Devices*, John Wiley & Sons, Inc., Hoboken, New Jersey, 1995, vol. 10.

3 P. Y. Yu and M. Cadorna, *Fundamentals of Seminconductors*, Springer, 4th edn, 2008.

4 J. Nelson, *The Physics of Solar Cells*, Imperial College Press, 2003.

5 P. Würfel, *Physics of Solar Cells: From Basic Principles to Advanced Concepts*, 2nd edn, Wiley-VCH Verlag GmbH & Co. KGaA, 2005.

6 F. A. Kroeger, *Chemistry of Imperfect Crystals*, North-Holland, Amsterdam, 1964.

7 J. Maier, *Angew. Chem., Int. Ed. Engl.*, 1993, **32**, 313–335.

8 D. Moia and J. Maier, *Mater. Horiz.*, 2023, **10**, 1641–1650.

9 T. Y. Yang, G. Gregori, N. Pellet, M. Grätzel and J. Maier, *Angew. Chem., Int. Ed.*, 2015, **54**, 7905–7910.

10 C. Eames, J. M. Frost, P. R. F. Barnes, B. C. O'Regan, A. Walsh and M. S. Islam, *Nat. Commun.*, 2015, **6**, 2–9.

11 A. Senocrate, I. Moudrakovski, G. Y. Kim, T.-Y. Yang, G. Gregori, M. Grätzel and J. Maier, *Angew. Chem., Int. Ed.*, 2017, **56**, 7755–7759.

12 N. Leupold, A. L. Seibel, R. Moos and F. Panzer, *Eur. J. Inorg. Chem.*, 2021, 2882–2889.

13 E. Ghahremanirad, S. Olyaee and J. Bisquert, *J. Phys. Chem. Lett.*, 2017, 1402–1406.

14 G. Y. Kim, A. Senocrate, T. Yang, G. Gregori, M. Grätzel and J. Maier, *Nat. Mater.*, 2018, **17**, 445–450.

15 D. Moia, I. Gelmetti, M. Stringer, O. Game, D. Lidzey, E. Palomares, P. Calado, J. Nelson, W. Fisher and P. R. F. Barnes, *Energy Environ. Sci.*, 2019, **12**, 1296–1308.

16 D. A. Egger, A. Bera, D. Cahen, G. Hodes, T. Kirchartz, L. Kronik, R. Lovrincic, A. M. Rappe, D. R. Reichman and O. Yaffe, *Adv. Mater.*, 2018, **30**, 1–11.

17 Y. Zhou, L. You, S. Wang, Z. Ku, H. Fan, D. Schmidt, A. Rusydi, L. Chang, L. Wang, P. Ren, L. Chen, G. Yuan, L. Chen and J. Wang, *Nat. Commun.*, 2016, **7**, 1–8.

18 Y. Rakita, I. Lubomirsky and D. Cahen, *Mater. Horiz.*, 2019, **6**, 1297–1305.

19 R. Merkle and J. Maier, *Phys. Chem. Chem. Phys.*, 2002, **4**, 4140–4148.

20 A. Senocrate, E. Kotomin and J. Maier, *Helv. Chim. Acta*, 2020, **103**, 1–8.

21 T. Defferriere, D. Klotz, J. C. Gonzalez-Rosillo, J. L. M. Rupp and H. L. Tuller, *Nat. Mater.*, 2022, **21**, 438–444.

22 G. Walch, B. Rotter, G. C. Brunauer, E. Esmaeili, A. K. Opitz, M. Kubicek, J. Summhammer, K. Ponweiser and J. Fleig, *J. Mater. Chem. A*, 2017, **5**, 1637–1649.

23 A. Viernstein, M. Kubicek, M. Morgenbesser, T. M. Huber, E. Ellmeyer, M. Siebenhofer, C. A. F. Vaz and J. Fleig, *Solid State Ionics*, 2022, **383**, 115992.

24 M. Morgenbesser, A. Schmid, A. Viernstein, J. De Dios Sirvent, F. Chiabrera, N. Bodenmüller, S. Taibl, M. Kubicek, F. Baiutti, A. Tarancon and J. Fleig, *Solid State Ionics*, 2021, **368**, 115700.

25 D. Meggiolaro, S. G. Motti, E. Mosconi, A. J. Barker, J. Ball, C. Andrea Riccardo Perini, F. Deschler, A. Petrozza and F. De Angelis, *Energy Environ. Sci.*, 2018, **11**, 702–713.

26 J. S. Park, J. Calbo, Y. K. Jung, L. D. Whalley and A. Walsh, *ACS Energy Lett.*, 2019, **4**, 1321–1327.

27 C. J. Tong, L. Li, L. M. Liu and O. V. Prezhdo, *J. Am. Chem. Soc.*, 2020, **142**, 3060–3068.

28 X. Zhang, M. E. Turiansky, J. X. Shen and C. G. Van De Walle, *Phys. Rev. B: Condens. Matter Mater. Phys.*, 2020, **101**, 140101.

29 S. Bitton and N. Tessler, *Energy Environ. Sci.*, 2023, **16**, 2621–2628.

30 D. Moia and J. Maier, *ACS Energy Lett.*, 2021, **6**, 1566–1576.

31 T. Kirchartz, J. A. Márquez, M. Stolterfoht and T. Unold, *Adv. Energy Mater.*, 2020, **10**, 1904134.

32 D. Barboni and R. A. De Souza, *Energy Environ. Sci.*, 2018, **11**, 3266–3274.

33 S. T. Birkhold, J. T. Precht, R. Giridharagopal, G. E. Eperon, L. Schmidt-mende and D. S. Ginger, *J. Phys. Chem. C*, 2018, **122**, 12633–12639.

34 A. Walsh, D. O. Scanlon, S. Chen, X. G. Gong and S. H. Wei, *Angew. Chem., Int. Ed.*, 2015, **54**, 1791–1794.

35 M. Von Smoluchowski, *Z. Phys. Chem.*, 1917, **92**, 129–168.

36 E. Kotomin and V. Kuzovkov, *Rep. Prog. Phys.*, 1992, **55**, 2079–2188.

37 J. Hu, Z. Xu, T. L. Murrey, I. Pelczer, A. Kahn, J. Schwartz and B. P. Rand, *Adv. Mater.*, 2023, **35**, 2303373.

38 X. Zhang, M. E. Turiansky, J.-X. Shen and C. G. Van De Walle, *Phys. Rev. B*, 2020, **101**, 140101.

39 Y. Zhou, I. Poli, D. Meggiolaro, F. De Angelis and A. Petrozza, *Nat. Rev. Mater.*, 2021, **6**, 986–1002.

40 Z. Xu, R. A. Kerner, L. Kronik and B. P. Rand, *ACS Energy Lett.*, 2024, **9**, 4645–4654.

41 A. Zohar, I. Levine, S. Gupta, O. Davidson, D. Azulay and O. Millo, *ACS Energy Lett.*, 2017, **2**, 2408–2414.

42 M. T. Neukom, A. Schiller, S. Züfle, E. Knapp, J. Ávila, D. Pérez-del-Rey, C. Dreessen, K. P. S. Zanoni, M. Sessolo, H. J. Bolink and B. Ruhstaller, *ACS Appl. Mater. Interfaces*, 2019, **11**, 23320–23328.

43 W. Clarke, L. J. Bennett, Y. Grudeva, J. M. Foster, G. Richardson and N. E. Courtier, *J. Comput. Electron.*, 2023, **22**, 364–382.

44 P. Calado, I. Gelmetti, B. Hilton, M. Azzouzi, J. Nelson and P. R. F. Barnes, *J. Comput. Electron.*, 2022, **21**, 960–991.

45 J. Bisquert, *Adv. Energy Mater.*, 2024, **2400442**, 1–35.

46 D. Moia, *Phys. Rev. Appl.*, 2025, **23**, 014055.

47 S. D. Stranks, G. E. Eperon, G. Grancini, C. Menelaou, M. J. P. Alcocer, T. Leijtens, L. M. Herz, A. Petrozza and H. J. Snaith, *Science*, 2013, **342**, 341–344.

48 M. C. Brennan, S. Draguta, P. V. Kamat and M. Kuno, *ACS Energy Lett.*, 2018, **3**, 204–213.

49 Y.-R. Wang, G. Yeong Kim, E. Kotomin, D. Moia and J. Maier, *J. Phys. Energy*, 2022, **4**, 011001.

50 A. Schiller, S. Jenatsch, B. Blülle, M. A. Torre Cachafeiro, F. Ebadi, N. Kabir, M. Othman, C. M. Wolff, A. Hessler-Wyser, C. Ballif, W. Tress and B. Ruhstaller, *J. Phys. Chem. Lett.*, 2024, **15**, 11252–11258.

51 G. Y. Kim, A. Senocrate, Y. Wang, D. Moia and J. Maier, *Angew. Chem., Int. Ed.*, 2021, **60**, 820–826.

52 A. Pockett, G. E. Eperon, N. Sakai, H. J. Snaith, L. M. Peter and P. J. Cameron, *Phys. Chem. Chem. Phys.*, 2017, **19**, 5959–5970.

53 D. A. Jacobs, H. Shen, F. Pfeffer, J. Peng, T. P. White, F. J. Beck and K. R. Catchpole, *J. Appl. Phys.*, 2018, **124** 225702.

54 W. White, C. D. Sanborn, R. S. Reiter, D. M. Fabian and S. Ardo, *J. Am. Chem. Soc.*, 2017, **139**, 11726–11733.

55 L. Schulte, W. White, L. A. Renna and S. Ardo, *Joule*, 2021, **5**, 2380–2394.